Institute of Theoretical Physics

University of Cologne

Time-Dependent Disorder in a Topological Insulator Realised with a Quantum Walk

Bachelor Thesis
Supervised by Prof. Dr. Achim Rosch
Second Referee Prof. Dr. Simon Trebst

Submitted by Jan Gelhausen
Matriculation Number 4878728

January 26, 2012
Cologne 2011/2012

Contents

1. Abstract

Demler et al. showed that modified versions of the discrete time quantum walk, *i.e.* the quantum mechanical analogue of the classical random walk, can function as quantum simulators for all topological phases classified in one and two dimensions [1]. Furthermore, they discussed the existence of robust edge modes, which are only present at the spatial boundary of a topological phase, and which account for the non-trivial topological character of the system.

In this Bachelor Thesis, the effect of both time-dependent and static disorder on the bound state of a one-dimensional topological insulator realised with a quantum walk are investigated both numerically and analytically. The motivation for this approach is that in an experimental set-up the sequence of unitary operations, which defines the quantum walk, is often realised imperfectly.

It is shown that the bound state of a one-dimensional topological insulator is insensitive to static disorder (energy conservation), whereas a time-dependent perturbation causes the bound state to decay (no conservation of energy). It can be observed that the bound states decay exponentially and that the decay constants scale quadratically with the strength of the disorder. In the long-time limit, the behaviour of the wave functions becomes diffusive.

A future prospect is the investigation of the behaviour of two-dimensional edge states realised on a square lattice with a quantum walk (Ref. [1]), which are subject to noise.

Zusammenfassung

Demler et al. haben gezeigt, dass modifizierte Versionen eines diskreten 'Quantum Walk', dem quantenmechanischen Analogon des klassischen 'Random Walk', als quanten Simulatoren für alle in ein und zwei Dimensionen klassifizierten topologischen Phasen dienen können [1]. Zusätzlich wurde die Existenz von robusten, lokalisierten Zuständen diskutiert, die sich nur an der Grenze unterschiedlicher topologischer Phasen aufzeigen. Ihre Existenz ist ein Beweis für den topologisch nicht trivialen Charakter des Systems.
In dieser Bachelorarbeit wird die Einwirkung von zeitabhängiger als auch zeitunabhängiger Störung auf den gebundenen Zustand in einem eindimensionalen topologischen Isolator, der mit Hilfe eines 'Quanten Walk' realisiert wird, numerisch als auch analytisch untersucht. Die Motivation für diese Vorgehensweise ist der Tatsache geschuldet, dass in einem experimentellen Aufbau die Sequenz von unitären Transformationen, die den 'Quanten Walk' definiert, nicht ideal realisiert werden kann.
Es wird gezeigt, dass der gebundene Zustand eines eindimensionalen topologischen Isolators robust gegenüber der Einwirkung von statischer Unordnung ist (Energierhaltung), wohingegen eine zeitabhängige Störung den gebundenen Zustand zerfallen lässt (keine Energieerhaltung). Es wird beobachtet, dass die gebundenen Zustände exponentiell zerfallen, wobei die Zerfallskonstanten quadratisch mit der Stärke der Unordnung skalieren. Für lange Zeiten wird das Verhalten der Wellenfunktion am gebundenen Zustand diffusiv.
In Zukunft ist die Untersuchung zweidimensionaler lokalisierter Zustände auf einem quadratischen Gitter, die mit Hilfe eines 'Quantum Walk' realisiert werden ([1]), unter dem Einfluss von zeitabhängiger als auch zeitunabhängiger Störung, geplant.

2. Motivation

This Bachelor Thesis is based on the ideas of Demler, Berg, Rudner and Kitagawa [1] who showed that quantum walks can realise and explore a wide range of dynamics of topologically distinct phases. They engineer a quantum walk in a way that allows it to support a topological phase transition in one and two dimensions, leading to the existence of topologically protected bound states. What is more, they showed that the discrete-time quantum walk is able to realise all ten possible symmetry classes in one and two dimensions. These classes can be distinguished by time-reversal symmetry, particle-hole symmetry and chiral symmetry [2].

The behaviour of quantum walks themselves is fascinating, because they turn out to be a powerful tool in quantum information science. The quantum walk is a quantum version of a classical random walk and is defined as a sequence of unitary operations. It nevertheless shows striking differences to its classical counterpart, employing the effects of superposition and coherent delocalisation of particles leading to interference phenomena.

Topological insulators (in 2D and 3D) were predicted theoretically in 2005 [4] and 2007 [5], prior to their first experimental discovery in 2007 [6], compare [7]. Topological insulators are new kinds of material in a sense that its quantum state of matter is characterised by topological invariances rather than by a local order parameter. These materials are insulating in their bulk, but can conduct electricity on their surface. These edge (2D) or surface (3D) states are non-accidental, because they are protected both by symmetry and topology; meaning that they cannot be destroyed by non-magnetic impurities or imperfections of the crystal.
Moreover, they are expected to host a lot of interesting features (*e.g.* charge fractionalisations or Majorana fermions [8] which are chargeless and their own antiparticles) and are thereby a field of intensive theoretical and experimental research.

The goal of this Bachelor Thesis is to analyse (both numerically and analytically) the behaviour of topologically protected states in 1D that are subject to noise.

Therefore, the Bachelor Thesis is structured as follows: The first chapter provides the reader with a short introduction to the general properties (definition, mathematical structure, idea) of a discrete-time quantum walk in 1D, since a modified protocol of the discrete-time protocol is used to realise topologically distinctive phases in the main part.

In the second part of the introduction, the reader is given a short overview of the properties of topological insulators, especially focusing on the difference of a topologically trivial (band)insulator and a non-trivial topological (band)insulator. Their first theoretical discovery in quantum Hall states is described as an example for the simplest two-dimensional topologically ordered state in order to convey the idea of topological notion. Furthermore, the abstract mathematical concept of topological invariants and its relation to the Berry phase, which provides a physical understanding of the idea of topological order, are briefly summarised.

As the topological character of the Hamiltonian of the split-step protocol is based on its symmetries that are described by the existence of antiunitary operators, the reader finds a short section about their properties. This is relevant, because these properties are necessary later on when the symmetry relations are derived.

In the fourth chapter, the theoretical concept of a split-step protocol is introduced, making it possible to realise topologically distinct phases. In the following sections its topological classification is derived and its consequences on the form of the energy spectrum are explained. Furthermore, it is described how the phase transition (realisation of different winding numbers) is enforced. The existence of the bound state (limited to phase boundaries) is numerically probed by the iteration of the split-step protocol.

The main part (Chapter 5) of the thesis investigates the behaviour of the bound states that are exposed to various forms of disorder (both dynamic and static). This is of particular interest for an experimental realisation of a quantum walk, where the system is inevitably subjected to noise or disorder.

In case of static disorder, the bound states are expected to persist, whereas in case of dynamic disorder the system's energy is not conserved and the states decay. It is of particular interest which function describes the decay best and how the processes of decay are related to the strength of disorder. This is investigated both numerically and analytically.

The seventh Chapter presents an outlook to a quantum walk in 2 dimensions realised on a square lattice [1]. Once again the existence of the surface states can be probed by numerical calculations with a modified version of the split-step quantum walk. Similar to the 1D case the surface states are non-accidental. It is of great interest to study their behaviour under disorder.

3. Introduction to Theoretical Concepts

3.1. Quantum Walk

In recent years, quantum walks have become increasingly important in the field of quantum information science with regard to efficient quantum algorithms. One hopes that a quantum computer can simulate a quantum walk to solve computational tasks more efficiently than with a classical random walk (*e.g.* discovery of satisfying assignments for Boolean formulae [9]).

The basic concept of a random walk is to shift the walker's current position according to the outcome of a (stochastic) coin-flip.

Classically, the walker's state can be described by a probability distribution in position-space. The random walk can be illustrated well by Galtons' Board (Quincunx, Fig. 3.1).

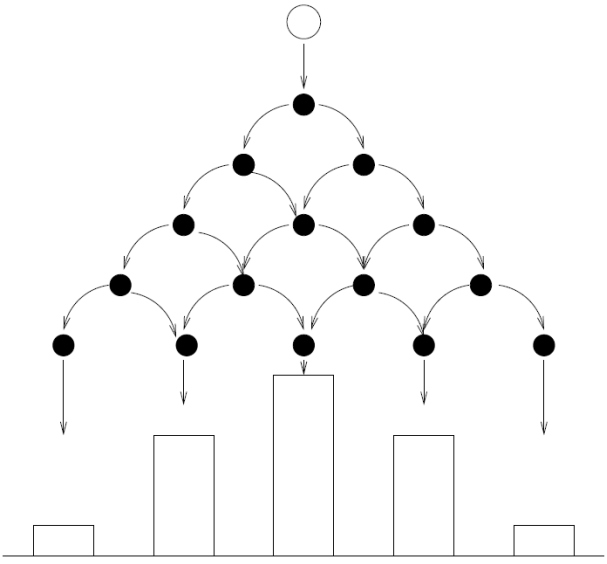

Figure 3.1.: Quincunx: A ball drops through an array of equally spaced pins which are arranged in rows and stuck in a board. At the bottom the balls are collected in slots. If there are N rows, each falling ball is a Bernoulli trial that consists of N steps. Because the ball is equally likely to bounce to the left or right, after many steps the binomial distribution (distribution of heights in the slot) converges to a Gaussian distribution with mean zero and variance $\sigma^2 = N$. Figure taken from [10]

A quantum (random) walk is the quantum analogue to its classical counterpart and defined as a sequence of unitary operations $\boldsymbol{U_i}$, see Ref.[10]. In case of a discrete random walk with N steps, it is defined as follows:

$$(\boldsymbol{U_1 \ldots U_m})^N = e^{-i\boldsymbol{\mathcal{H}}t}, \quad \text{for } t = \Delta t N \tag{3.1}$$

The operator $\boldsymbol{\mathcal{H}}$ is the Hamiltonian of the system. The key idea is to iterate a sequence of unitary operations $\boldsymbol{U_i}$ on an initial state $|\Psi_0\rangle$ for a time t and measure the resulting probability distribution over a d-dimensional lattice, see Ref. [9]. Quantum walks can simulate the behaviour of other quantal systems, *e.g.* topologically distinct phases of a topological insulator.

In order to implement a non-trivial quantum version of the random walk one needs two degrees of freedom. The internal degree of freedom of the system can be realised by the spin of a particle that takes the role of the coin. The external degree of freedom is the particle's position in space. In this Thesis the quantum walk will be defined on a line (1D) and on a square-lattice (2D) with grid-length 1. In order to realise a discrete-time quantum walk, the states of the total system are described in the Hilbert space $\mathcal{H} = \mathcal{H}_C \otimes \mathcal{H}_P$, where $\mathcal{H}_C = \{|\uparrow\rangle, |\downarrow\rangle\}$ and $\mathcal{H}_P = \{|x\rangle\,; x \in \mathbb{Z}\}$. The flipping of the coin can be implemented by a unitary (coin) operator that acts only on the internal degree of freedom of the system. The outcome of the operation determines the direction of the walker's next step. This can be achieved by introducing a spin-dependent unitary translation operator $\boldsymbol{T}$ that shifts both spins into opposite directions. Here, the coin-operator corresponds to the rotation matrix $\mathbf{R}(\theta)$ of a spin-$\frac{1}{2}$ particle acting only in the Hilbert space of $\mathcal{H}_C$ (a rotation about the y-axis by an angle θ).

$$\mathbf{R}(\theta) = \exp\left(\frac{i}{2}\theta\boldsymbol{\sigma}_y\right) = \begin{pmatrix} \cos(\frac{\theta}{2}) & -\sin(\frac{\theta}{2}) \\ \sin(\frac{\theta}{2}) & \cos(\frac{\theta}{2}) \end{pmatrix} \tag{3.2}$$

The shifting operator $\boldsymbol{T}$ is defined as follows:

$$\boldsymbol{T}_{\uparrow,\downarrow} = \sum_x |x+1\rangle\langle x| \otimes |\uparrow\rangle\langle\uparrow| + |x-1\rangle\langle x| \otimes |\downarrow\rangle\langle\downarrow| \tag{3.3}$$

The quantum walk with N steps is defined by the sequence of unitary operations $\boldsymbol{U}$ acting on the wave-function:

$$\boldsymbol{U}^N = (\boldsymbol{T}_{\uparrow,\downarrow} \cdot (\boldsymbol{R}(\theta) \otimes \mathbb{1}_k))^N \tag{3.4}$$

The operator $\boldsymbol{U}$ entangles both degrees of freedom of the system because the translation $\boldsymbol{T}_{\uparrow,\downarrow}$ delocalises the particle over two lattice sites by bringing the system into a superposition of positions. This ultimately leads to the possibility of constructive and destructive interference in subsequent steps, whereas in a classical random walk each path lives on its own. This feature gives rise to a completely different behaviour of the quantum walk compared to its classical counterpart. The probability distribution of a quantum walk does not converge to a limiting distribution and, in general, is highly sensitive to the walker's initial state and the specific coin-operators. The quantum random walk is reversible and therefore its initial state can be reconstructed by the application of $\boldsymbol{U^{-1}}$.
A modified version of a quantum walk, the split-step quantum walk, (discussed by Demler et al. [1]) is used in this Thesis in order to realise a topological phase transition that ultimately results in the presence of a bound state near the phase-transition point.

3.2. Trivial and Non-Trivial Topological Insulators

Trivial Topological Insulators

A trivial insulator does not conduct any electricity. It can be described within the general framework of band theory of solids and is well understood. It has finite numbers of unoccupied bands and no partially occupied bands. The conduction band is separated from the valence band by a large energy gap.

Non-Trivial Topological Insulators

In the 1980's the discovery of the integer quantum Hall effect gave rise to new organisational principles of quantum matter. In the quantum Hall state, electrons confined to a 2D plane and exposed to a strong magnetic field perpendicular to the electrons' motion circulate in quantised orbits with quantised levels of energy (Landau levels). Along the edges the electrons form so-called 'skipping orbits', where they circulate in one direction only, which depends on the orientation of the applied magnetic field. This means that the electron gas is insulating in its bulk (Landau levels), but conducts electricity at the edges. The topological invariant is the quantized Hall conductance that counts the number of edge states ($\sigma_{xy} = n\frac{e^2}{h}$). The prominent feature of the edge states is, that they persist even in the presence of impurities meaning that they are not accidental surface states. Their presence is protected by the concepts of topology.
Actually, the existence of edge states does not necessarily depend on the presence of an external magnetic field.

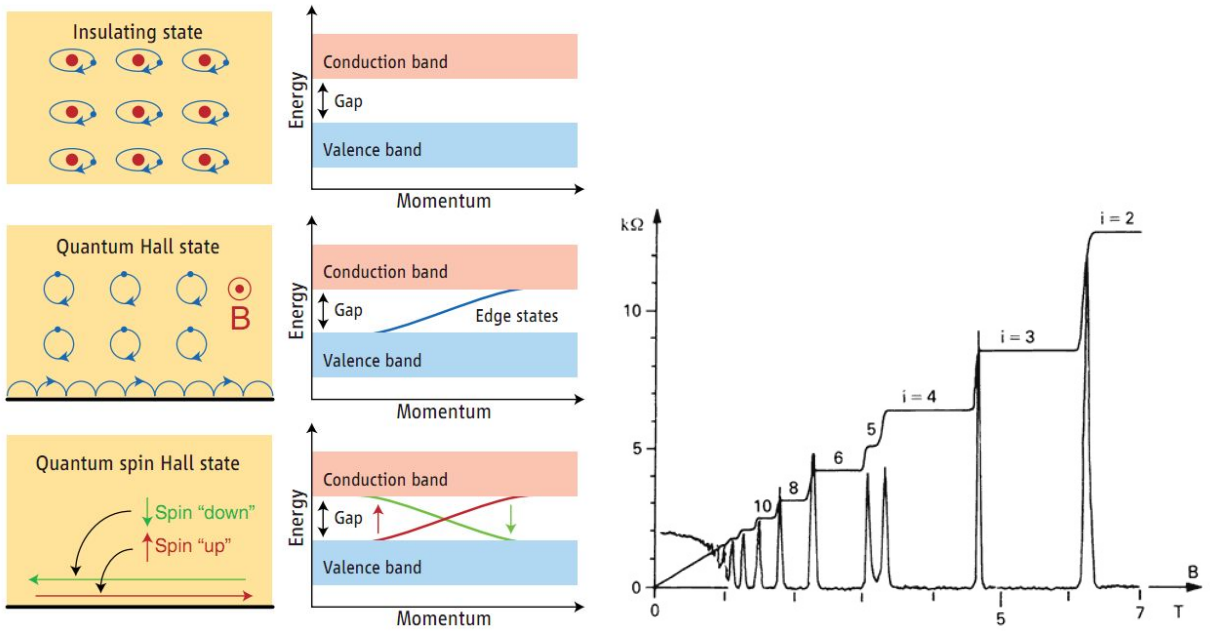

Figure 3.2.: **Top:** Sketch of a trivial insulator. The electrons are well-localised in orbits. An energy gap separates the conduction and the valence band.
Middle: The quantum Hall state as a non-trivial insulator. Due to the presence of an external magnetic field the electrons in the middle of the material move in closed orbits. At the edges, the electrons bounce off the surface but there is no possibility for a change in direction since it is determined by the orientation of the magnetic field. The material will not conduct electricity in its bulk but does so along the edges. Since charge flows in one direction only (chiral edge states) and the edges of the sample are far apart, scattering processes of the electrons are strongly suppressed. Quantum Hall states require the presence of a magnetic field which breaks time-reversal symmetry. The quantized Hall conductivity is an integer topological invariant.
Bottom: Quantum spin Hall effect. An energy-gap is present due to strong spin-orbit coupling. Electricity is conducted through spin-polarized helical edge states. Figure taken from [11]
Right: A quantized Hall conductance is observed in quantum Hall systems. $\sigma_{xy} = n\frac{e^2}{h}$ (plateaus). The lower peaked curves represent the logitudinal resistance ρ_{xx} that vanishes at each plateau. Figure taken from [12]

It turned out that spin-orbit coupling can be strong enough to take over the role of the external magnetic field. The locking of the direction of the spin and its movement leads to spin-polarised counter-propagating edge states (quantum spin Hall effect, see Ref. [7],[13],[14]). These materials are now called topological insulators.

Topological insulators are new states of condensed matter and can also be understood within the framework of band theory of solids. A topological insulator is a material that is insulating in its bulk but, in contrast to an ordinary insulator, has protected edge (2D) or surface (3D) states. These surface states occur only at topological phase boundaries, and therefore originate from topological invariants which do not change as long as the material remains insulating in its bulk. This is often referred to as the bulk-boundary correspondence, because the existence of surface or edge states follows from topological properties of the bulk.

Usually, the explanation of phase transitions from disordered into ordered states of matter is based on the Landau theory of second-order phase transitions, which characterises states of condensed matter by different local order parameters. According to Landau theory, a continuous phase transition is accompanied by a spontaneously broken symmetry as well as a change in value of the local order parameters. For example, a crystal spontaneously breaks translation and rotation symmetries of space, superconductors break U(1) gauge symmetries for charged particles and are classified by their critical temperature T_C as their local order parameter. The concept of describing a topological phase transition with the help of local order parameter fails, because symmetries are preserved.

A new classification of ordered states of condensed matter is based upon topological invariants of the examined system rather than on local order parameters. In Mathematics, 2D topological manifolds are, for example, characterised by an integer number that arises as an integral of its closed surface (Gauss-Bonnet Theorem). The topological classification is based upon the manifold's genus (g), which counts the number of holes. Accordingly, a torus is topologically different ($g = 1$) from a sphere ($g = 0$) (see Ref. [15]) The topological character of a system remains unchanged under smooth or adiabatic deformations of the manifold. A simple illustration for a changing (unchanging) topological notion can be found in Fig. 3.3. A doughnut and a coffee cup belong to the same topological equivalence class as they can be transformed into each other without cutting their surfaces. In physics, smooth deformations are applied to the Hamiltonian and therefore affect its spectrum. Topologically, semiconductors and trivial insulators are equivalent because one can transform the one into the other by tuning the Hamiltonian so as to interpolate continuously between the two without closing their energy gap (see Ref. [17] page 2). In their simplest form, equivalence classes of Hamiltonians can be distinguished by a topological invariant $n \in \mathbb{Z}$, called Chern number (similar to the genus of the surface in mathematics).

Physically, this invariant can be understood in terms of the Berry phase (see Ref. [18], and Ref. [17] page 3). The Berry phase is a well defined irreducible, geometric phase in quantum mechanics, which is obtained by the wave function on a closed loop in momentum space given an adiabatic deformation of the Hamiltonian. Here 'adiabatic' means that the time evolution of an eigenstate of the system is only determined by a dynamical phase and a geometrical phase (Berry phase), *i.e.* the system remains in its time-dependent eigenstate without making transitions into different states. For example, a particle moving in momentum space encircling the 1D Brillouin Zone picks up the Berry phase which can be expressed in terms of the Bloch wave-functions $|u(\vec{k})\rangle$ as:

$$n_m = \frac{1}{2\pi i} \int_{\partial BZ} dk \, \langle u_m(\vec{k})| \, \nabla_k \, |u_m(\vec{k})\rangle \tag{3.5}$$

Using Stokes' Theorem and $A = -i \, \langle u_m(\vec{k})| \, \nabla_k \, |u_m(\vec{k})\rangle$ this may also be expressed as a surface integral:

$$n_m = \frac{1}{2\pi} \int_{BZ} d^2k \, (\nabla_k \times A) \tag{3.6}$$

$\nabla \times A$ is called the Berry curvature. Summing over all occupied bands m, one obtains the total Chern number n as the topological invariant of the system, provided that there exists an energy gap separating a finite number of occupied and unoccupied bands.

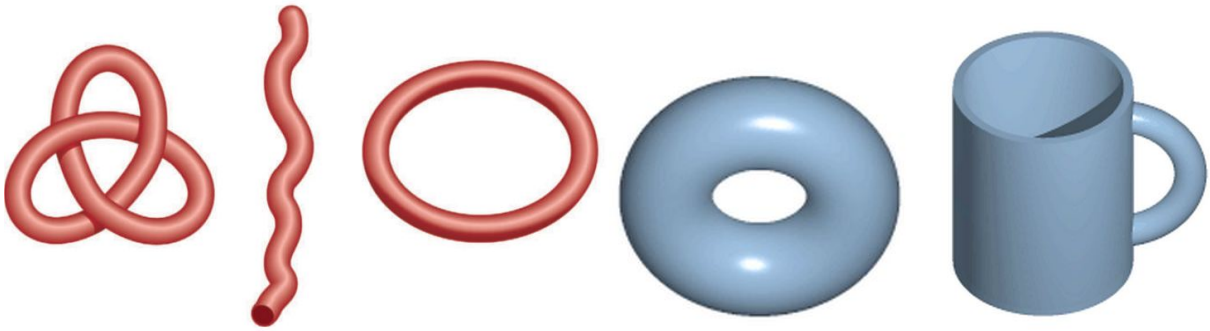

Figure 3.3.: **(Left)** The trefoil knot has got a different topological number than the closed loop **(Right)**.This is because neither of them can be transformed into the other without having to cut the wire **(Centre)**. Figure obtained from [16]. This is in contrast to the transformation of a doughnut into a coffee cup. These manifolds are topologically equivalent because there exists a sequence of transformations that transforms the one into the other without cutting their surfaces.

For a 2×2 Hamiltonian of the form $\mathcal{H} = \sum_k E(\vec{k})\vec{n}(\vec{k}) \cdot \vec{\sigma}$ (see Eq. 4.6), the topological invariant can also be expressed as:

$$n = \frac{1}{4\pi} \int_{BZ} d^2k \left(\vec{n} \cdot (\partial_{k_z} \vec{n} \times \partial_{k_y} \vec{n}) \right) \tag{3.7}$$

, (see Ref. [17]). The Chern number n can geometrically be interpreted as the number of times the unit vector $\vec{n}$ wraps around the unit sphere as $\vec{k}$ is taken through the Brillouin zone (the closed loop in parameter space). The Berry flux is then related to the solid angle enclosed by the unit vector $\vec{n}$.

In other words, the Brillouin zone takes the role of the surface, and the Berry phase provides its curvature. Hence, the the electron's wave functions are in some way 'knotted'.

3.2.1. Topological Invariant in 2D Time-Reversal Invariant Systems

The quantum spin Hall state exhibits a different topological invariant than the quantum Hall state. The Hall conductivity changes its sign under time-reversal, meaning that it is always zero in the quantum spin Hall state. Nevertheless, there exists a different topological invariant $\mathbb{Z}_2$ in systems with time-reversal symmetry that can only take two possible values ($\nu = 0$ and $\nu = 1$). For inversion symmetric systems, for example, it can be determined by the parity of the Bloch wave functions at special points in the Brillouin zone (see Ref. Kane et al. [17]).

3.3. Antiunitary Operators

The symmetries of the Hamiltonian discussed in Chapter 4.3.1 are defined by the existence of antiunitary operators. Therefore it is necessary to define their properties.
An operator $\boldsymbol{A}$ is considered antiunitary if it satisfies the following relations:

$$\boldsymbol{A}(\alpha\,|\Psi\rangle + \beta\,|\Psi\rangle) = \alpha^*\boldsymbol{A}\,|\Psi\rangle + \beta^*\boldsymbol{A}\,|\Psi\rangle \tag{3.8}$$

$$\langle \boldsymbol{A}\Psi|\boldsymbol{A}\Phi\rangle = \langle\Psi|\Phi\rangle^* = \langle\Phi|\Psi\rangle \tag{3.9}$$

An antiunitary operator satisfies the equation $\boldsymbol{A}\boldsymbol{A}^\dagger = \mathbb{1}$. To see this note that:

$$|\boldsymbol{A}\,|\Psi\rangle\,|^2 = \langle \boldsymbol{A}\Psi|\boldsymbol{A}\Psi\rangle = (\langle\Psi|\,\boldsymbol{A}^\dagger\boldsymbol{A}\,|\Psi\rangle)^* \overset{!}{=} \langle\Psi|\Psi\rangle \tag{3.10}$$

And for $\langle\Phi|\Psi\rangle = 0 \Rightarrow \langle\Phi|\,\boldsymbol{A}^\dagger\boldsymbol{A}\,|\Psi\rangle = 0$.
The product of a unitary operator $\boldsymbol{U}$ and an antiuntiary operator $\boldsymbol{A}$ is also antiunitary. This follows from Eq. (3.8) and Eq. (3.9):

$$\boldsymbol{U}\boldsymbol{A}(\alpha\Psi + \beta\Psi) = \boldsymbol{U}(\alpha^*\boldsymbol{A}\Psi + \beta^*\boldsymbol{A}\Psi) = \alpha^*\boldsymbol{U}\boldsymbol{A}\Psi + \beta^*\boldsymbol{U}\boldsymbol{A}\Psi \tag{3.11}$$

$$\langle \boldsymbol{U}\boldsymbol{A}\Psi|\boldsymbol{U}\boldsymbol{A}\Phi\rangle = \langle \boldsymbol{A}\Psi|\,\boldsymbol{U}^\dagger\boldsymbol{U}\,|\boldsymbol{A}\Phi\rangle \overset{(3.9)}{=} \langle\boldsymbol{A}\Psi|\boldsymbol{A}\Phi\rangle \overset{(3.9)}{=} \langle\Phi|\Psi\rangle \tag{3.12}$$

The complex conjugate of an antiunitary operator that consists of a unitary and an antiunitary operator is:

$$\boldsymbol{B} = \boldsymbol{U}\boldsymbol{A} \Rightarrow \boldsymbol{B}^\dagger = (\boldsymbol{U}\boldsymbol{A})^\dagger = \boldsymbol{A}^\dagger\boldsymbol{U}^\dagger \tag{3.13}$$

This becomes evident from:

$$\langle\Psi|\boldsymbol{U}\boldsymbol{A}\Phi\rangle = \Big\langle \boldsymbol{U}^\dagger\Psi|\boldsymbol{A}\Phi\Big\rangle = \Big(\Big\langle \boldsymbol{A}\Phi|\boldsymbol{U}^\dagger\Psi\Big\rangle\Big)^* = \langle\Phi|\,\boldsymbol{A}^\dagger\boldsymbol{U}^\dagger\,|\Psi\rangle \tag{3.14}$$

$$\langle\Psi|\boldsymbol{B}\Phi\rangle = \Big\langle\Phi|\boldsymbol{B}^\dagger|\Psi\Big\rangle \tag{3.15}$$

$$\Rightarrow \boldsymbol{B}^\dagger = (\boldsymbol{U}\boldsymbol{A})^\dagger = \boldsymbol{A}^\dagger\boldsymbol{U}^\dagger \tag{3.16}$$

In particular, the complex conjugation $\boldsymbol{K}$ is antiunitary, because

$$\boldsymbol{K}(\alpha\,|\Psi\rangle + \beta\,|\Psi\rangle) = \alpha^*\boldsymbol{K}\,|\Psi\rangle + \beta^*\boldsymbol{K}\,|\Psi\rangle \tag{3.17}$$

$$\langle \boldsymbol{K}\Psi|\boldsymbol{K}\Phi\rangle = \langle\Psi^*|\Phi^*\rangle = \int dx^3\Psi\Phi^* = \langle\Phi|\Psi\rangle \tag{3.18}$$

The time-reversal symmetry operator $\boldsymbol{\mathcal{T}}$ is defined by the equation:

$$e^{-i\mathcal{H}t}\boldsymbol{\mathcal{T}}e^{-i\mathcal{H}t}\left|\Psi(0)\right\rangle = \boldsymbol{\mathcal{T}}\left|\Psi(0)\right\rangle \tag{3.19}$$

At the time t a time-reversal operation is performed. The resulting state of the system is further developed for a time period t. If the system at $t = 0$ is in its time-reversed state, the Hamiltonian is considered invariant under the operations performed by $\boldsymbol{\mathcal{T}}$ (see Ref.[19] page 228).

After differentiating Eq.(3.19) at $t = 0$ it follows that:

$$\boldsymbol{\mathcal{T}}i\boldsymbol{\mathcal{H}} = -i\boldsymbol{\mathcal{H}}\boldsymbol{\mathcal{T}} \tag{3.20}$$

$$\Rightarrow [\boldsymbol{\mathcal{T}}, \boldsymbol{\mathcal{H}}] = 0 \Leftrightarrow \boldsymbol{\mathcal{T}}\boldsymbol{\mathcal{H}}\boldsymbol{\mathcal{T}}^{-1} = \boldsymbol{\mathcal{H}} \tag{3.21}$$

4. Investigation of Topological Phases with a Quantum Walk in 1D

4.1. The Split-Step Protocol

The one-dimensional discrete-time quantum protocol (DTQW) is given by the unitary evolution operator $\boldsymbol{U}$:

$$\boldsymbol{U} = (\boldsymbol{T}_{\uparrow,\downarrow} \cdot (\boldsymbol{R}(\theta) \otimes \mathbb{1}_x)) \tag{4.1}$$

$$\boldsymbol{R}(\theta) = \exp\left(\frac{i}{2}\theta \cdot \sigma_y\right) = \begin{pmatrix} \cos(\frac{\theta}{2}) & -\sin(\frac{\theta}{2}) \\ \sin(\frac{\theta}{2}) & \cos(\frac{\theta}{2}) \end{pmatrix} \tag{4.2}$$

$$\boldsymbol{T}_{\uparrow,\downarrow} = \sum_x |x+1\rangle\langle x| \otimes |\uparrow\rangle\langle\uparrow| + |x-1\rangle\langle x| \otimes |\downarrow\rangle\langle\downarrow| \tag{4.3}$$

The rotation matrix $\boldsymbol{R}(\theta)$ rotates the system around the y-axis by an angle θ. The translation operator $\boldsymbol{T}$ is a spin-dependent shift on a 1D line with integer grid-length. It delocalises particles of opposite spin in different directions by one lattice site.

In order to observe a non-trivial topological character of the system, a split-step protocol (STQW) is introduced that enforces the system to undergo a phase transition which manifests itself in the presence of a robust edge state at the phase boundary.

The split-step protocol defines a set of Hamiltonians $\boldsymbol{\mathcal{H}_{ss}}(\theta_1, \theta_2(x))$ that only depends on the particular choice of the pairs of rotation angles (θ_1, θ_2).

The split-step protocol is defined by:

$$\boldsymbol{U}_{ss}(\theta_1, \theta_2(x)) = \boldsymbol{T}_{\downarrow}\boldsymbol{R}(\theta_2(x))\boldsymbol{T}_{\uparrow}\boldsymbol{R}(\theta_1) \tag{4.4}$$

The shift operator $\boldsymbol{T}$ has been altered in a way that it separately shifts the spin-up (spin-down) component of the walker to the right (left) by one lattice site.

The dynamics of the system are governed by the sequence of unitary operations $\boldsymbol{U_{ss}}(\theta_1, \theta_2(x))$,

which can be written in a more convenient way as:

$$\boldsymbol{U_{ss}}(\theta_1, \theta_2(x)) = \exp\left(-i\boldsymbol{\mathcal{H}_{ss}}(\theta_1, \theta_2(x))\delta t\right), \quad \hbar = 1 \tag{4.5}$$

$$\boldsymbol{\mathcal{H}_{ss}}(\theta_1, \theta_2(x)) = \int_{-\pi}^{\pi} dk[E_\theta(k)\vec{n}_\theta(k) \cdot \vec{\boldsymbol{\sigma}}] \otimes |k\rangle \langle k| \tag{4.6}$$

$$\vec{\boldsymbol{\sigma}} = (\boldsymbol{\sigma_x}, \boldsymbol{\sigma_y}, \boldsymbol{\sigma_z}) \tag{4.7}$$

The STQW protocol is a discrete quantum walk, therefore the systems time-evolution is limited to unit intervals δt. Consequently, the eigenvalues of the Hamiltonian $\pm E_{(\theta_1,\theta_2)}$ are only defined modulo 2π, resulting in a quasi-energy spectrum. The split-step protocol was suggested and discussed by Demler et al. [1].

4.2. Energies and Eigenstates

By application of the Fourier transformation for the translation operator $\boldsymbol{T}_{\uparrow,\downarrow}$, one obtains the following expression in the basis of Fourier modes:

$$\begin{aligned}
\boldsymbol{T}_\uparrow &= \sum_x |x+1\rangle \langle x| \otimes |\uparrow\rangle \langle\uparrow| + |x\rangle \langle x| \otimes |\downarrow\rangle \langle\downarrow|, \quad \text{with} \quad |x\rangle = \sum_k \frac{1}{\sqrt{2\pi}} e^{ikx} |k\rangle \\
&= \sum_{k,k'} \left(\left(\underbrace{\sum_x \frac{1}{2\pi} e^{i(k-k')x}}_{\delta(k-k')} \right) |k\rangle \langle k'| e^{ik} \otimes |\uparrow\rangle \langle\uparrow| + \left(\underbrace{\sum_x \frac{1}{2\pi} e^{i(k-k')x}}_{\delta(k-k')} \right) |k\rangle \langle k'| \otimes |\downarrow\rangle \langle\downarrow| \right) \\
&= \sum_k \left(|k\rangle \langle k| e^{ik} \otimes |\uparrow\rangle \langle\uparrow| + |k\rangle \langle k| \otimes |\downarrow\rangle \langle\downarrow| \right) \\
&= \sum_k |k\rangle \langle k| \otimes \begin{pmatrix} e^{ik} & 0 \\ 0 & 1 \end{pmatrix} \\
&\text{chosen basis:} \quad \{|\uparrow\rangle, |\downarrow\rangle\} = \left\{ \begin{pmatrix} 1 \\ 0 \end{pmatrix}, \begin{pmatrix} 0 \\ 1 \end{pmatrix} \right\}
\end{aligned}$$

After a similar procedure for $\boldsymbol{T}_\downarrow$ the matrix representation of the DTQW protocol is

$$\begin{aligned}
&\boldsymbol{U_{ss}}(\theta_1, \theta_2(x)) = \sum_k |k\rangle \langle k| \otimes \\
&\begin{pmatrix} e^{ik}\cos\left(\frac{\theta_1}{2}\right)\cos\left(\frac{\theta_2}{2}\right) - \sin\left(\frac{\theta_1}{2}\right)\sin\left(\frac{\theta_2}{2}\right) & -e^{ik}\sin\left(\frac{\theta_1}{2}\right)\cos\left(\frac{\theta_2}{2}\right) - \sin\left(\frac{\theta_2}{2}\right)\cos\left(\frac{\theta_1}{2}\right) \\ \cos\left(\frac{\theta_1}{2}\right)\sin\left(\frac{\theta_2}{2}\right) + e^{-ik}\sin\left(\frac{\theta_1}{2}\right)\cos\left(\frac{\theta_2}{2}\right) & -\sin\left(\frac{\theta_1}{2}\right)\sin\left(\frac{\theta_2}{2}\right) + e^{-ik}\cos\left(\frac{\theta_1}{2}\right)\cos\left(\frac{\theta_2}{2}\right) \end{pmatrix}
\end{aligned}$$

Writing the Hamiltonian in a convenient parametrization in momentum-space

$$\boldsymbol{\mathcal{H}} = \sum_k \vec{L}(k, \theta_1, \theta_2) \cdot \vec{\boldsymbol{\sigma}} \tag{4.8}$$

where the eigenvalues are given by $E(k) = \pm|\vec{L}(k, \theta_1, \theta_2)|$, one has to write $\boldsymbol{U_{ss}}$ in terms of the Pauli matrices:

$$\begin{aligned}
\boldsymbol{U_{ss}} &= c_0 \mathbb{1} + \sum_{i=1}^{3} c_i \cdot \boldsymbol{\sigma_i} \\
\boldsymbol{U_{ss}\sigma_j} &= c_0 \mathbb{1}\boldsymbol{\sigma_j} + \sum_{i=1}^{3} c_i \left(\delta_{ij}\mathbb{1} + i \sum_{k=1}^{3} \epsilon_{ijk}\boldsymbol{\sigma_k} \right) \\
&= c_0 \mathbb{1}\boldsymbol{\sigma_j} + c_j \mathbb{1} + i \sum_{k,i=1}^{3} \epsilon_{ijk}\boldsymbol{\sigma_k} \\
\Rightarrow c_j &= \frac{1}{2}\mathrm{Tr}(\boldsymbol{U_{ss}\sigma_j}) \\
&\{j = 0, 1, 2, 3 \quad , \boldsymbol{\sigma_0} = \mathbb{1} \quad , \mathrm{Tr}(\boldsymbol{\sigma}_{j\neq 0}) = 0\}
\end{aligned}$$

The explicit expression for the energies is obtained by comparing coefficients in the following equation:

$$\begin{aligned}
\boldsymbol{U_{ss}} &= c_0 \mathbb{1} + \vec{c} \cdot \vec{\boldsymbol{\sigma}} \\
&\stackrel{!}{=} \exp\left(-i \sum_k \vec{R}_{\theta_1,\theta_2}(k) \cdot \vec{\boldsymbol{\sigma}} \otimes |k\rangle \langle k| \right) \\
&= \exp\left(-i \sum_k E_{\theta_1,\theta_2}(k) \vec{n}_{\theta_1,\theta_2}(k) \cdot \vec{\boldsymbol{\sigma}} \otimes |k\rangle \langle k| \right) \\
&= \sum_k \cos(E_{\theta_1,\theta_2}(k)) \mathbb{1} - i \sin(E_{\theta_1,\theta_2}(k)) \vec{n} \cdot \vec{\boldsymbol{\sigma}} \otimes |k\rangle \langle k| \\
\Rightarrow \vec{n} &= i \frac{1}{\sin(E_{\theta_1,\theta_2}(k))} \vec{c}, \quad \cos(E_{\theta_1,\theta_2}(k)) = c_0
\end{aligned}$$

The coefficients for the Hamiltonian are:

$$\cos(E_{\theta_1,\theta_2}(k)) = \cos(\theta_2/2)\cos(\theta_1/2)\cos(k) - \sin(\theta_1/2)\sin(\theta_2/2) \tag{4.9}$$

$$\tag{4.10}$$

$$n_x(k) = \frac{\cos(\theta_2/2)\sin(\theta_1/2)\sin(k)}{\sin(E_{\theta_1,\theta_2}(k))}$$

$$n_y(k) = \frac{\cos(\theta_1/2)\sin(\theta_2/2) + \cos(k)\cos(\theta_2/2)\sin(\theta_1/2)}{\sin(E_{\theta_1,\theta_2}(k))} \tag{4.11}$$

$$n_z(k) = \frac{-\cos(\theta_2/2)\cos(\theta_1/2)\sin(k)}{\sin(E_{\theta_1,\theta_2}(k))} \tag{4.12}$$

The angle θ_2 can be regarded as the tuning parameter for the energy spectrum when keeping $\theta_1 = -\frac{\pi}{2}$ fixed. The resulting band structure is shown in Fig. 4.1. Note that there is a gap closing for a value of $\theta_2 = \frac{\pi}{2}$.

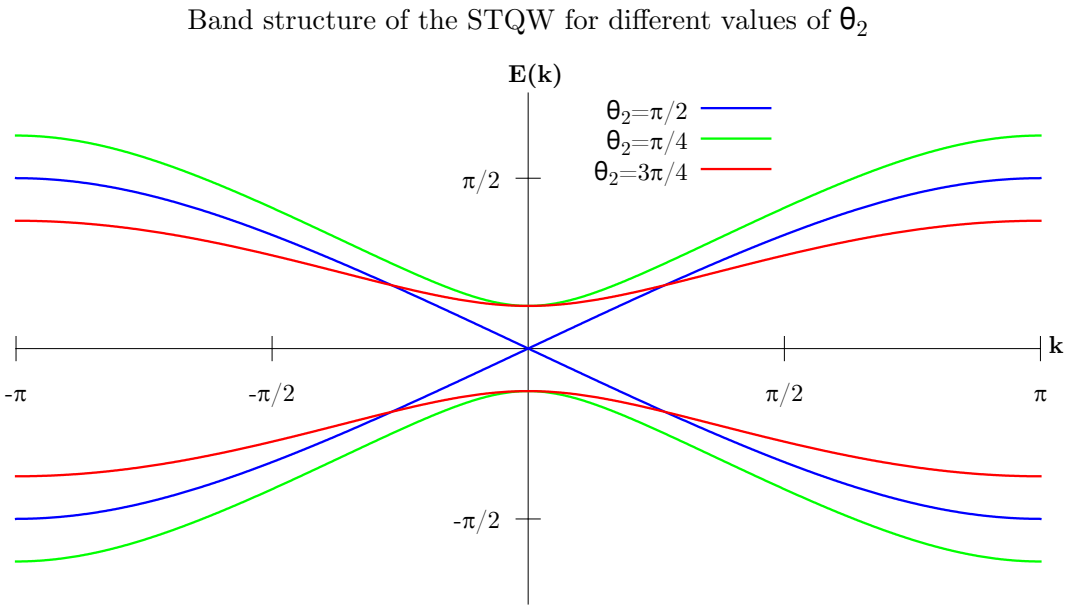

Figure 4.1.: Band structure for the STQW for different values of θ_2 ($\theta_1 = -\pi/2$). Note that the gap closing at $\theta_2 = \frac{\pi}{2}$ marks the point of the topological phase transition for the split-step-protocol at $k = 0$ in the phase space. In general, the energies are only defined modulo 2π, and the gap closings always occur at $k = 0, \pm n\pi$ with energies $E = 0, n\pi$, $n \in \mathbb{N}$.
Time-reversal symmetry and particle-hole symmetry of the split-step protocol guarantee that the spectrum is symmetric with respect to the momentum and energy axes.

4.3. Topological Classification of the STQW

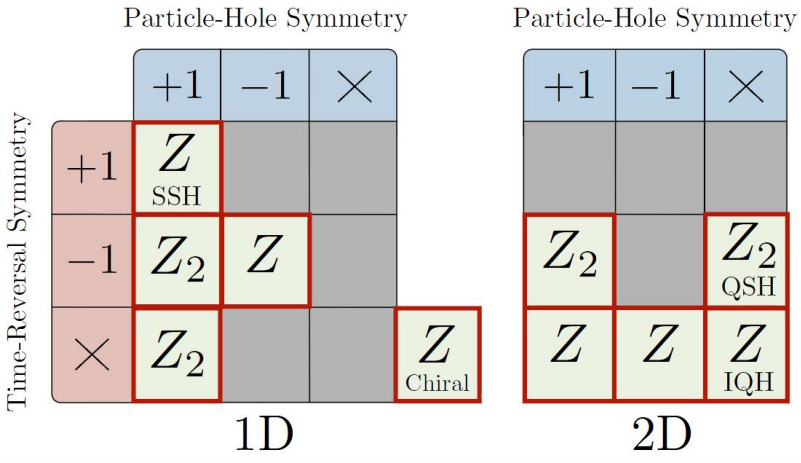

Figure 4.2.: Table of topological insulators in one (1D) and two (2D) dimensions. Time-reversal symmetry (TRS) and particle-hole symmetry (PHS) are defined by the existence of **antiunitary** operators $\boldsymbol{\mathcal{T}}$ and $\boldsymbol{\mathcal{P}}$ satisfying the equations $\boldsymbol{\mathcal{T}}^2 = \pm 1, \boldsymbol{\mathcal{P}}^2 = \pm 1$. In the absence of both TRS and PHS, a distinct chiral symmetry with a **unitary** $\boldsymbol{\Gamma}$ satisfying equation may be found. In each case, the symmetry-allowed phases are classified by an integer ($\mathbb{Z}$) or binary ($\mathbb{Z}_2$) topological invariant. Caption (adapted) and figure taken from [1].

The class of topological phases that can be realised is determined by two features of the system. Firstly, by its dimensionality and, secondly, by the symmetries of the Hamiltonian, (see Fig. 4.2). The classification is based upon the presence or absence of symmetry operators. In two-dimensional systems, time-reversal symmetry and particle-hole symmetry can be present with $\boldsymbol{\mathcal{T}}^2 = \boldsymbol{\mathcal{P}}^2 = \pm 1$. Together with a chiral symmetry $\boldsymbol{\Gamma}$ one ends up with 10 possible symmetry classes in 2D, see Ref. [2],[13].

Since the relevant symmetry operators of the STQW both square to 1, $\boldsymbol{\mathcal{T}}^2 = \boldsymbol{\mathcal{P}}^2 = 1$, the symmetry class of the system is labelled "SSH" (Su-Shrieffer-Heger-Model, see Ref.[20]) by Demler, Berg, Rudner, Kitagawa. The table for the classification of the topological phases is shown in Fig. 4.2.

4.3.1. Symmetries of the Hamiltonian

The Hamiltonian of the STQW has time-reversal symmetry (TRS), particle-hole symmetry (PHS) and a chiral symmetry (CS). It thus satisfies:

$$\boldsymbol{\mathcal{T}}\boldsymbol{\mathcal{H}}_{ss}\boldsymbol{\mathcal{T}}^{-1} = \boldsymbol{\mathcal{H}}_{ss} \quad \text{(TRS)} \tag{4.13}$$

$$\boldsymbol{\mathcal{P}}\boldsymbol{\mathcal{H}}_{ss}\boldsymbol{\mathcal{P}}^{-1} = -\boldsymbol{\mathcal{H}}_{ss} \quad \text{(PHS)} \tag{4.14}$$

$$\boldsymbol{\Gamma}_{\theta_2}^{-1}\boldsymbol{\mathcal{H}}_{ss}\boldsymbol{\Gamma}_{\theta_2} = -\boldsymbol{\mathcal{H}}_{ss} \quad \text{(CS)} \tag{4.15}$$

Since symmetry operators have to be either unitary or antiunitary (Wigner's Theorem) there are no unitary operators that satisfy (TRS) and (PHS) for the STQW.

4.3.1.1. Particle-Hole Symmetry

PHS is satisfied by the antiunitary operator $\boldsymbol{\mathcal{P}} = \boldsymbol{K}$, where $\boldsymbol{K}$ is the complex conjugation operator. The Operator $\boldsymbol{U_{ss}}$ of the STQW-protocol (see Eq. (4.4)) is real. Regarding Eq. (4.5) this implies $\boldsymbol{\mathcal{H}}_{ss}^{*} = -\boldsymbol{\mathcal{H}}_{ss}$.

Since $\boldsymbol{\mathcal{P}}\boldsymbol{\mathcal{H}} + \boldsymbol{\mathcal{H}}\boldsymbol{\mathcal{P}} = 0$ for every energy eigenfunction $|n\rangle$ with $\boldsymbol{\mathcal{H}}|n\rangle = E_n|n\rangle, \boldsymbol{\mathcal{P}}|n\rangle$ is a valid solution with energy $-E_n$. As a consequence, eigenvalues E_n and $-E_n$ always appear in pairs for each k.

4.3.1.2. Chiral Symmetry

The chiral symmetry is given by an operator

$$\boldsymbol{\Gamma}^{\pm 1} = \exp\left(\mp i\pi/2\vec{A}_{\theta_1} \cdot \vec{\boldsymbol{\sigma}}\right) = \mathbb{1}\cos(\pi/2) \mp i\vec{A}_{\theta_1} \cdot \vec{\boldsymbol{\sigma}}\sin(\pi/2) = \mp i\vec{A}_{\theta_1} \cdot \vec{\boldsymbol{\sigma}} \tag{4.16}$$

$$\vec{A}_{\theta_1} = (\cos(\theta_1/2), 0, \sin(\theta_1/2)) \tag{4.17}$$

where $\vec{A}_{\theta_1}$ is perpendicular to the vector $\vec{n}(k)$ for all k.

The presence of chiral symmetry (Eq.(4.15)) under $\mathbf{\Gamma}$ and $\vec{A}$ can be verified:

$$\begin{aligned}
\mathbf{\Gamma}^{-1}\boldsymbol{\mathcal{H}}_{ss}\mathbf{\Gamma} &= \int_{-\pi}^{\pi} dkE(k)(\vec{A}_{\theta_1}\cdot\vec{\boldsymbol{\sigma}})(\vec{n}\cdot\vec{\boldsymbol{\sigma}})(\vec{A}_{\theta_1}\cdot\vec{\boldsymbol{\sigma}})\otimes|k\rangle\langle k| \qquad (4.18)\\
&\overset{(4.19)}{=} -i\int_{-\pi}^{\pi} dkE(k)(\vec{A}_{\theta_1}\cdot\vec{\boldsymbol{\sigma}})(\vec{A}_{\theta_1}\times\vec{n})\cdot\vec{\boldsymbol{\sigma}}\otimes|k\rangle\langle k|\\
&\overset{(4.20)}{=} -i\int_{-\pi}^{\pi} dkE(k)(\vec{A}_{\theta_1}\cdot\vec{\boldsymbol{\sigma}})(\vec{A}_{\theta_1}\cdot\vec{n}) - i\vec{A}^2(\vec{n}\cdot\vec{\boldsymbol{\sigma}})\otimes|k\rangle\langle k|\\
&= -\int_{-\pi}^{\pi} dkE(k)(\vec{n}\cdot\vec{\boldsymbol{\sigma}})\otimes|k\rangle\langle k|\\
&= -\boldsymbol{\mathcal{H}}_{ss}
\end{aligned}$$

$$\begin{aligned}
(\vec{n}\cdot\vec{\boldsymbol{\sigma}})(\vec{A}_{\theta_1}\cdot\vec{\boldsymbol{\sigma}}) &= \sum_{ij} n_iA_j\boldsymbol{\sigma}_i\boldsymbol{\sigma}_j = \sum_{ij} n_iA_j\left(\delta_{ij}\mathbb{1} + i\sum_k \epsilon_{ijk}\boldsymbol{\sigma}_k\right) \qquad (4.19)\\
&= \left(\sum_{ij} n_iA_j\delta_{ij}\right)\mathbb{1} - i\sum_k\left(\sum_{ij}\epsilon_{jik}A_jn_i\right)\boldsymbol{\sigma}_k\\
&= \mathbb{1}\left(\vec{A}_{\theta_1}\cdot\vec{n}\right) - i\left(\vec{A}_{\theta_1}\times\vec{n}\right)\cdot\vec{\boldsymbol{\sigma}}\\
&\overset{\vec{A}\perp\vec{n}}{=} -i\left(\vec{A}_{\theta_1}\times\vec{n}\right)\cdot\vec{\boldsymbol{\sigma}}
\end{aligned}$$

$$\begin{aligned}
(\vec{A}_{\theta_1}\cdot\vec{\boldsymbol{\sigma}})(\vec{A}_{\theta_1}\times\vec{n})\cdot\vec{\boldsymbol{\sigma}} &= \left(\sum_l A_l\boldsymbol{\sigma}_l\right)\left(\sum_k\left(\sum_{ij}\epsilon_{ijk}A_in_j\right)\boldsymbol{\sigma}_k\right) \qquad (4.20)\\
&= \sum_{lijk}\epsilon_{ijk}A_lA_in_j\boldsymbol{\sigma}_l\boldsymbol{\sigma}_k = \sum_{lijk}\epsilon_{ijk}A_lA_in_j\left(\delta_{lk}\mathbb{1} + i\sum_m\epsilon_{lkm}\boldsymbol{\sigma}_m\right)\\
&= \mathbb{1}\sum_k\left(\sum_{ij}\epsilon_{ijk}A_in_j\right)A_k + i\sum_{ijlm}\left(\sum_k\epsilon_{kij}\epsilon_{kml}\right)A_lA_in_j\boldsymbol{\sigma}_m\\
&= \mathbb{1}(\vec{A}_{\theta_1}\times\vec{n})\cdot\vec{A}_{\theta_1} + i\sum_{ijlm}\delta_{im}\delta_{jl}A_lA_in_j\boldsymbol{\sigma}_m - i\sum_{ijlm}\delta_{il}\delta_{jm}A_lA_in_j\boldsymbol{\sigma}_m\\
&\overset{\vec{A}\perp(\vec{A}\times\vec{n})}{=} i\left(\sum_i A_i\boldsymbol{\sigma}_i\right)\left(\sum_j A_jn_j\right) - i\left(\sum_i A_iA_i\right)\left(\sum_j n_j\boldsymbol{\sigma}_j\right)\\
&= i(\vec{A}_{\theta_1}\cdot\vec{\boldsymbol{\sigma}})(\vec{A}_{\theta_1}\cdot\vec{n}) - i\vec{A}^2(\vec{n}\cdot\vec{\boldsymbol{\sigma}})\\
&\overset{\vec{A}\perp\vec{n}}{=} -i(\vec{n}\cdot\vec{\boldsymbol{\sigma}})
\end{aligned}$$

4.3.1.3. Time-Reversal Symmetry

TRS of $\boldsymbol{\mathcal{H}}_{ss}$ is guaranteed by the existence of chiral symmetry and PHS with $\boldsymbol{\mathcal{T}} = \boldsymbol{\Gamma}\boldsymbol{\mathcal{P}}$ which is a antiunitary operator:

$$\boldsymbol{\mathcal{T}}\boldsymbol{\mathcal{H}}_{ss}\boldsymbol{\mathcal{T}}^{-1} = \boldsymbol{\Gamma}\boldsymbol{\mathcal{P}}\boldsymbol{\mathcal{H}}_{ss}\boldsymbol{\mathcal{P}}^{-1}\boldsymbol{\Gamma}^{-1} = \boldsymbol{\mathcal{H}}_{ss} \tag{4.21}$$

If $|\Psi(k)\rangle$ is a solution to Schrödinger's equation with energy $E(k)$, its time-reversed state $\boldsymbol{\mathcal{T}}|\Psi(k)\rangle$ is also a solution to Schrödinger's equation with the same energy $E(-k) = E(k)$.

Together TRS and PHS guarantee that the energy spectrum $E(k)$ is symmetric with respect to both the momentum axis and the energy axis (see Fig. 4.1).

4.3.2. Enforcing the Phase Transition – The Winding Number

As chiral symmetry forces $\vec{n}_{\theta_1,\theta_2}(k)$ to lie in a plane perpendicular to $\vec{A}_{\theta_1}$, the corresponding topological invariant is the number of times that $\vec{n}_{\theta_1,\theta_2}(k)$ winds around the origin (see Fig. 4.3). The band structure is made of the energy eigenvalues $E(k)$ which, in the case of the STQW for a fixed θ_1, depends only on θ_2. One can interpret θ_2 as the tuning parameter for the Hamiltonian that interpolates continuously between the band structure without closing the energy gap, *i.e.* without changing the topological character of the system (*e.g.* the winding number). The split-step Hamiltonian $\boldsymbol{\mathcal{H}}_{ss}$ realises topological phases with winding numbers $Z = 0$ and $Z = 1$. These phases are separated by phase transition lines, where the energy gap of the system vanishes. In the STQW, this is the case for $k = 0$ with $\theta_1 = -\frac{\pi}{2}$ and with $\theta_2 = \frac{\pi}{2}$ (see Fig. 4.1). In order to realize a surface state of a topological insulator, an inhomogeneous system with $Z = 0$ on the left hand side and $Z = 1$ on the right hand side is investigated. The spatial boundary between these two topological phases is enforced by a site-dependent spin rotation matrix $\boldsymbol{R}(\theta_2(x))$, where $\theta_2(x)$ is chosen to be:

$$\theta_2(x) = \frac{1}{2}(\theta_{2-} + \theta_{2+}) + \frac{1}{2}(\theta_{2+} - \theta_{2-})\tanh(x/3) \tag{4.22}$$

$$\theta_2(x) = \begin{cases} \theta_{2-}, & x \gg 0 \\ \theta_{2+}, & x \ll 0 \end{cases}$$

If the rotation angles $(\theta_{2+}, \theta_{2-})$ are chosen with a fixed θ_1 to realise distinct topological phases in the asymptotic limit ($x \gg 0$ and $x \ll 0$), a bound state exists near the phase boundary at $x = 0$. The existence of the bound state does not depend on the specific

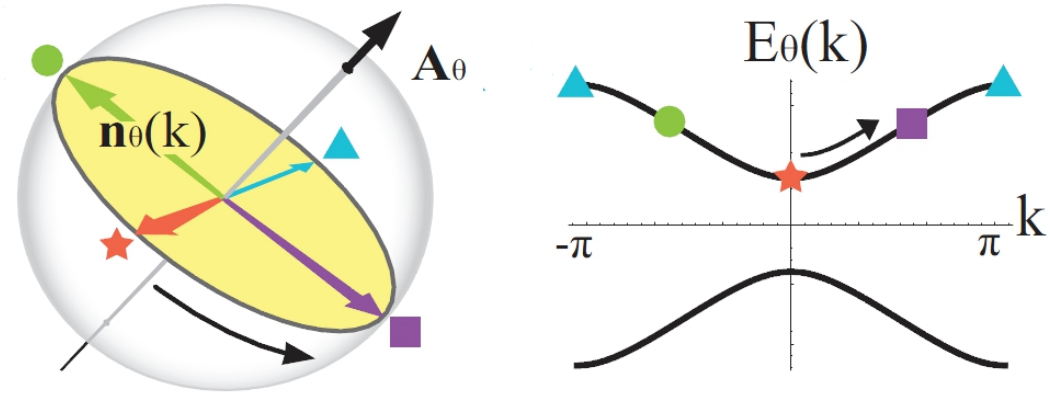

Figure 4.3.: The band structure is plotted for the 1D DTQW with $\theta_1 = \frac{\pi}{2}$. The vector $\vec{n}(k)$ winds around the origin as k traverses the Brillouin zone from $-\pi$ to π. For the DTQW, the winding number is always 1. For the STQW, the winding number depends on the particular choice of $\theta(x)$. $\vec{A}_\theta$ is perpendicular to $\vec{n}(k)$ for all k. Corresponding points in the figures are marked. Figure taken from Ref.[1].

shape of the $\theta_2(x)$-function and is guaranteed by topology. In fact, the bound state is stable against weak perturbations that do not change the systems topological character.

4.4. Determination of the Topological Phase-Diagram

In order to determine the phase-diagram for the STQW, one has to calculate the number of times the vector $\vec{n}$ wraps around the unit sphere. If $\vec{A}$ is rotated in the direction of the z-axis, $\vec{n}$ will lay in the xy-plane for all k. With $\tilde{\vec{n}} = \boldsymbol{R}_y(\frac{\theta_1}{2})\vec{n}$, the expression for the winding number Z is given by a line integral of the form:

$$Z = \oint \frac{x}{r^2} dy - \frac{y}{r^2} dx \tag{4.23}$$

$$Z = \frac{1}{2\pi} \int_{-\pi}^{\pi} \frac{1}{\tilde{\vec{n}}^2} \left(\tilde{n}_x \partial_k \tilde{n}_y - \tilde{n}_y \partial_k \tilde{n}_x \right) dk \tag{4.24}$$

since the polar coordinate θ is related to the rectangular coordinates x, y as:

$$d\theta = \frac{1}{r^2}(x dy - y dx) \quad \text{with} \quad r^2 = x^2 + y^2 \tag{4.25}$$

A numerical evaluation of Eq. (4.24) for $\theta_1, \theta_2 \in [-2\pi, 2\pi]$ gives the phase-diagram for the STQW, that can be found in Fig. 4.4

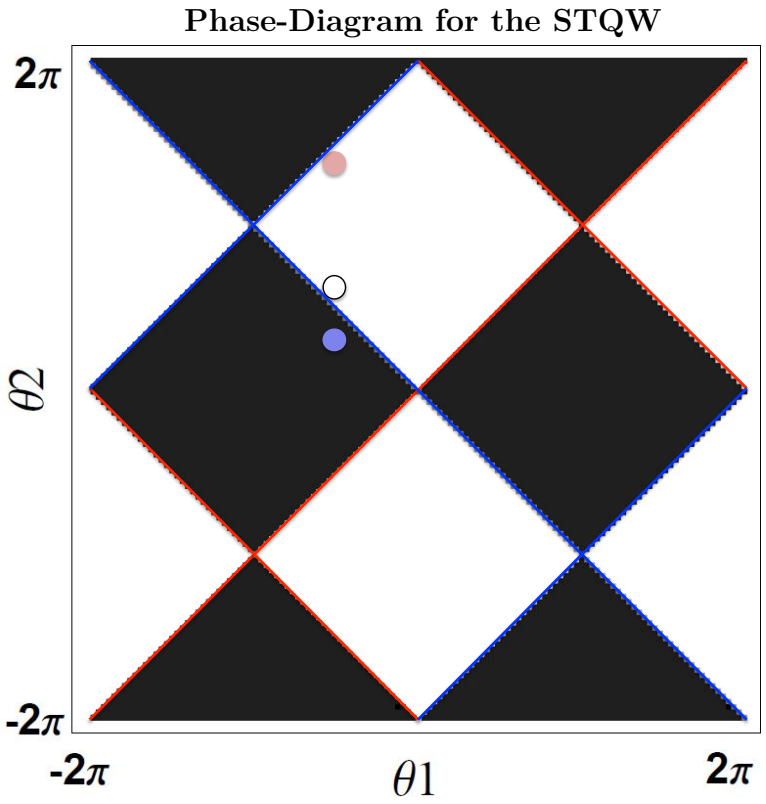

Figure 4.4.: Phase diagram for the STQW from numerical evaluation of Eq. (4.24), screened with intervals of 0.1 width. Black regions correspond to winding number 1, white regions correspond to winding number 0.
At the red (blue) lines, the energy-gap closes at an energy $E = \pi$ ($E = 0$). The dots in the panel correspond to the choices of $\theta_{2+} = \frac{11\pi}{8}$ (coral dot), $\theta_{2+} = \frac{\pi}{4}$ (blue dot), $\theta_{2-} = \frac{3\pi}{4}$ (white dot) with a fixed $\theta_1 = -\frac{\pi}{2}$. The colors correspond to Fig. 4.5.

4.5. The Bound State – Non-Trivial Topological Character of the System

By placing the quantum walker directly onto one of the phase boundaries and iterating the STQW protocol, the existence of the topologically protected bound state can be verified. If the initial state has a non-zero overlap with the bound state, a part of the wave function is expected to remain localized at $x = 0$. Numerical calculations are shown in Fig. 4.5.

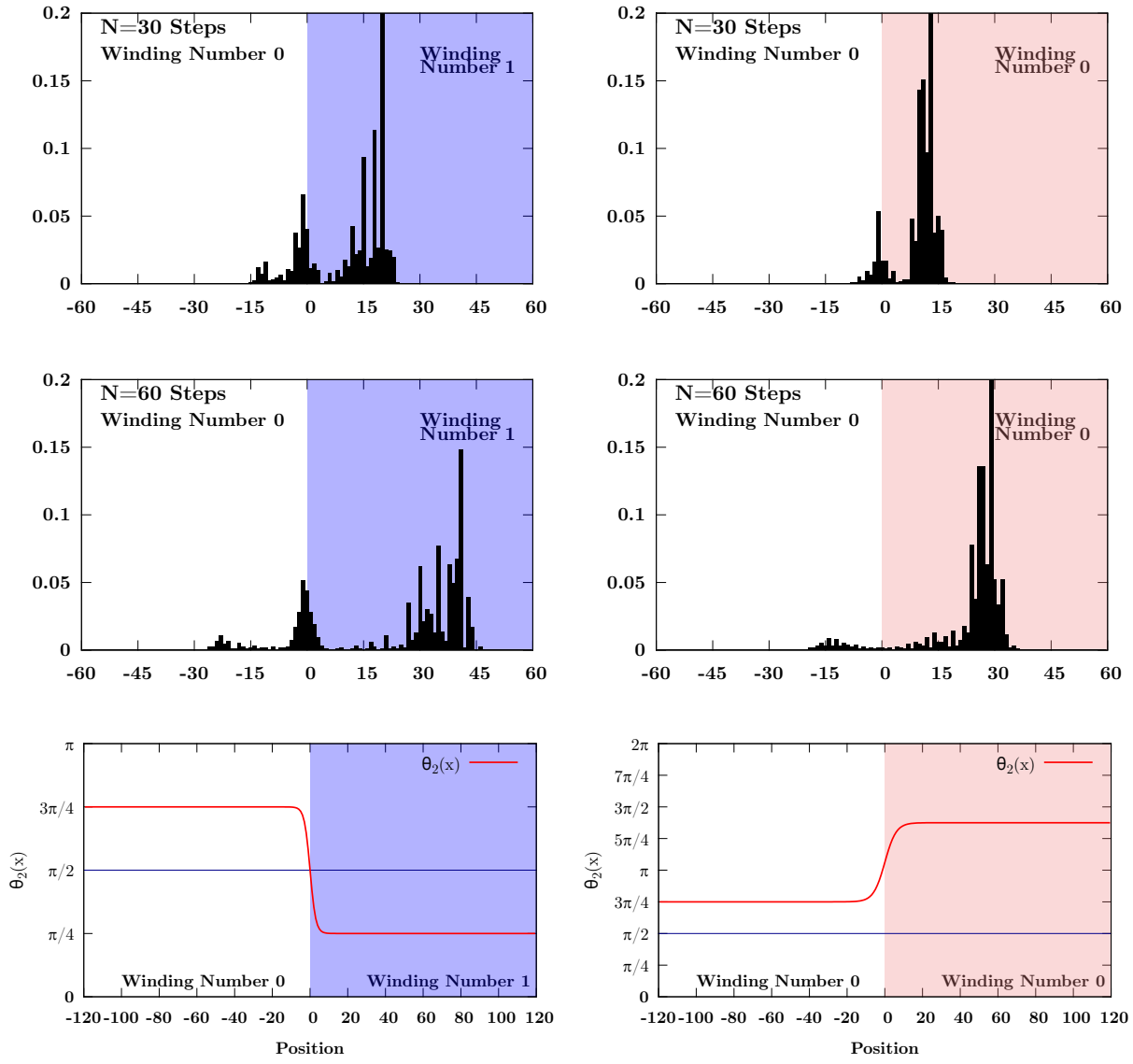

Figure 4.5.: The y-axes of the upper four pictures show the weight of the wave functions $|\Psi|^2$. Note that the specific shape of the probability functions highly depends on the choice of the initial wave function (except for the presence or absence of the bound state). In all figures the initial wave function is $|\Psi\rangle_0 = |0\rangle \otimes |\uparrow\rangle$. The majority of the wave function is moving right.
Left: The existence of the bound state has been verified using the split-step protocol with parametric values $\theta_1 = -\frac{\pi}{2}, \theta_{2-} = \frac{3\pi}{4}, \theta_{2+} = \frac{\pi}{4}$.
Right: The probability for the walker to be located around $x = 0$ goes to zero in subsequent steps if $\theta_{2+} = \frac{11\pi}{8}$. In the absence of the phase boundary there is no bound state.

5. Exposing the Bound State to Disorder

5.1. Static Disorder (Energy Conservation)

The effect of static disorder on the bound state at the interface of topologically distinct phases is examined. Theoretically, one expects the bound state to remain stable against weak perturbations. A perturbation is considered as weak as long as it does not change the topological character of the system, which in the 1D case of the split-step quantum walk (STQW) means that the winding number is not altered. Because there are no nearby states inside the bulk energy gap, the static disorder will conserve the energy of the system. Furthermore, it is expected that the existence of the bound states is not sensitive to the explicit details of the form of the boundary.

The $\theta_2(x)$-function (Eq. (4.22)), which enforces the closing of the gap in the system and thereby guarantees the existence of the robust edge states, is slightly modified by another function $\gamma(x)$, which returns uncorrelated random numbers at each integer lattice site:

$$\widetilde{\theta}_2(x) = \theta(x)_2 + \delta\gamma(x) \tag{5.1}$$

$$\gamma(x) \in [-1, 1] \tag{5.2}$$

δ corresponds to the strength of the disorder, $\gamma(x)$ is a uniform random distribution. The modified θ-function is shown in Fig. 5.1. Note that for each step of the STQW the same disordered $\tilde{\theta}_2$-function is used. The localised state of the system is centred around $x = 0$, which corresponds to $\theta_2(0) = \frac{\pi}{2}$. The effect of static disorder on the bound state can be seen in Fig. 5.2.

The bound state remains stable against the perturbation. This reveals the non-trivial topological character of the system and shows that the surface state is not 'accidental', but guaranteed by the topological notion of the system.

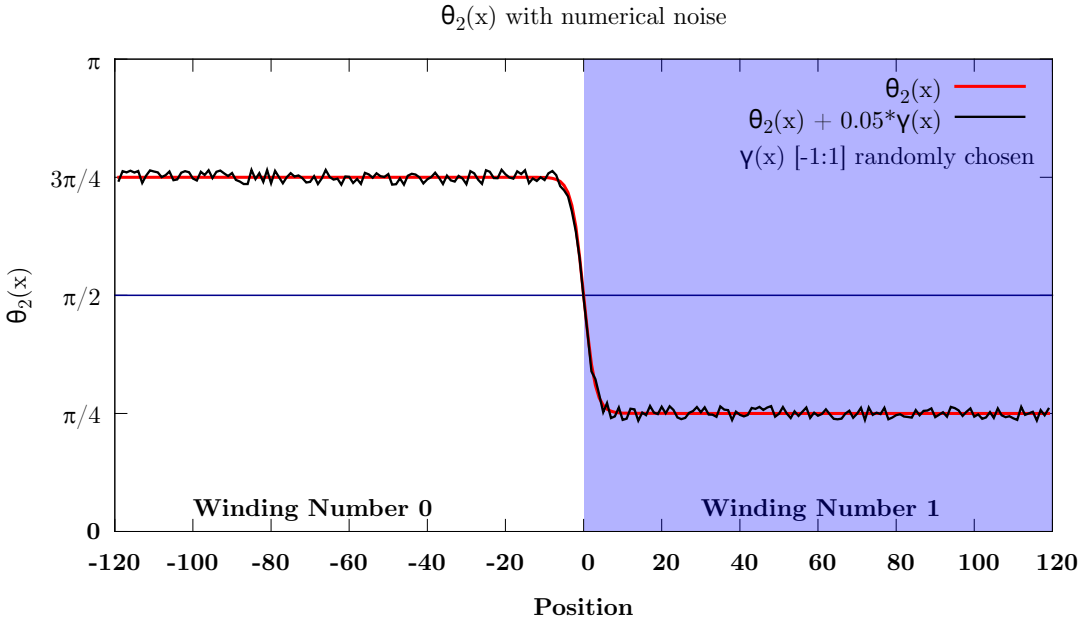

Figure 5.1.: One possible realisation of disorder with the help of uncorrelated uniformly distributed random numbers ($\langle x_i x_{i+1} \rangle = 0$). The strength of the disorder is choosen to be $\delta = 0.05$.
In the **static** case the disorder configuration is fixed whereas in the case of **dynamic disorder** it changes within subsequent iterations of the split-step protocol.

5.2. Dynamic Disorder (No Energy Conservation)

In an experimental setup (*e.g.* Quantum Walk in Position Space with Single Optically Trapped Atoms Ref. [21], see also Ref. [22]), the sequence of unitary operations for a quantum walk may not be realised perfectly. It is of great interest to investigate a system in the presence of slight mistakes of the unitary operations, *i.e.* a system subject to time-dependent noise.
The bound state localised at $x = 0$ with the split-step protocol and the state-dependent rotation angle $\theta_2(x)$ are topologically protected and expected to persist in the presence of weak perturbations. The specific shape of the $\theta_2(x)$ is unimportant for the presence of the bound state as long as there is a phase transition. However, if the shape of the $\theta_2(x)$-function is altered with the help of random numbers inducing a time-dependent numerical noise (see Fig. 5.1), the Hamiltonian of the system becomes time-dependent. As a result, there is no conservation of energy, and the bound state is expected to decay

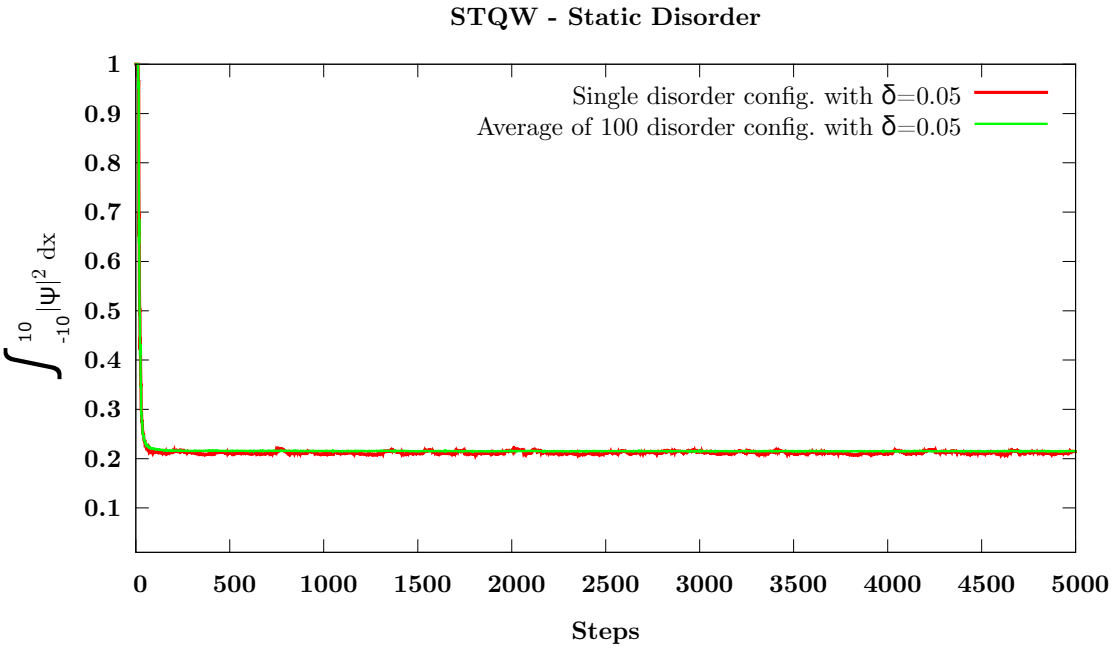

Figure 5.2.: The effect of static disorder on the bound state.
The bound sate remains stable against the perturbation, which is in agreement with the theory. The error bars are included.

within subsequent iterations of the split-step protocol.

$$\tilde{\theta_2}(x,t) = \theta_2(x) + \delta\gamma(x,t) \tag{5.3}$$
$$\gamma(x,t) \in [-1:1] \quad \text{randomly choosen}$$
$$\delta \quad \text{disorder parameter}$$

The strength of the disorder is controlled by a parameter δ chosen between 0 (no disorder) and 0.30 (strong disorder). $\gamma(x,t)$ is a uniform time-dependent random distribution.

For the numerical analysis of the behaviour of the bound states subject to disorder, $|\Psi|^2$ is integrated over a small range (depending on the particular choice of θ_2) around the phase-transition point $x = 0$, for different values of the disorder strength δ and for each iteration of the STQW protocol.

It is expected that in the presence of fluctuating disorder the bound states decay exponentially. With increasing strength of the disorder parameter δ the behaviour of these curves is dominated by stochastic noise. Therefore one has to take the average over multiple

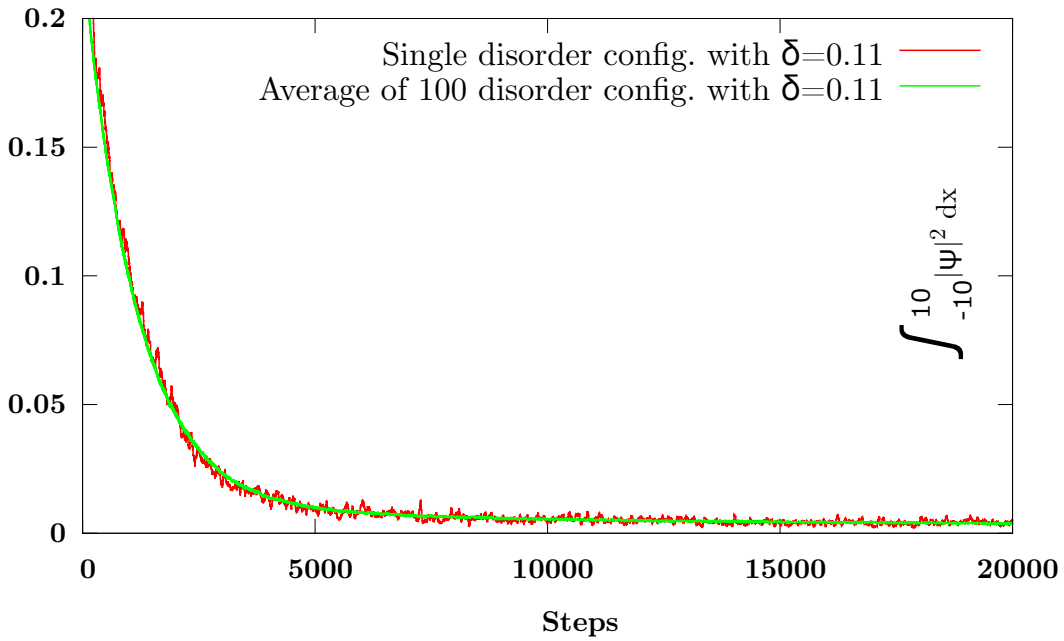

Figure 5.3.: The shape of the red curve is dominated by the effects of stochastic noise. Averaging over N disorder configurations suppresses the noise by a factor of $\sqrt{N}$. The plot includes errorbars.

realisations of disorder configurations for the $\theta_2(x,t)$ function for each curve to get appropriate estimates for the decay functions. The number of disorder realisations that have been chosen depend on the particular strength of disorder (see Table 5.1). The averaging procedure is carried out every time a decay-function is fitted. The errorbars represent the standard deviation. The noise can be suppressed by a factor of $\sqrt{N}$, where N is the number of disorder configurations (Central Limit Theorem). This can be seen in Fig. 5.3. As the bound states are expected to decay exponentially, the specific decay time constants prove to be of particular interest. Therefore, the decay curves are fitted with a function $f(x) = ae^{-bx}$. In order to guarantee that only the decay of the non-vanishing overlap of the initial wave function ($|\Psi\rangle = |0\rangle \otimes |\uparrow\rangle$) with the bound state is taken into account, the

δ	Disorder Configurations
<0.04	10
(0.04-0.08)	50
>0.08	100

Table 5.1.: Disorder Realisations for various values of disorder δ.

fitting process is started after 100 iterations of the STQW protocol, so that the unbound part of the wave function traverses out of the area of integration (compare Fig. 4.5). In a plot with logarithmic scale on the y-axis the decay curves are expected to be linear and of the form $\log(f(x)) = \log(a) - bx$. In Fig. 5.5 it can be seen that the decay of the bound state divides up into different parts. In a limited region (depending on the strength of the disorder and the number of steps) the curves decay exponentially. For many iterations of the STQW protocol, deviations from the exponential decay and the numerically calculated results become visible. The behaviour of the bound state can then be described by laws of diffusion. These regions are called 'diffusive tails'.

Figure 5.4.: Exposing the bound states to dynamic disorder

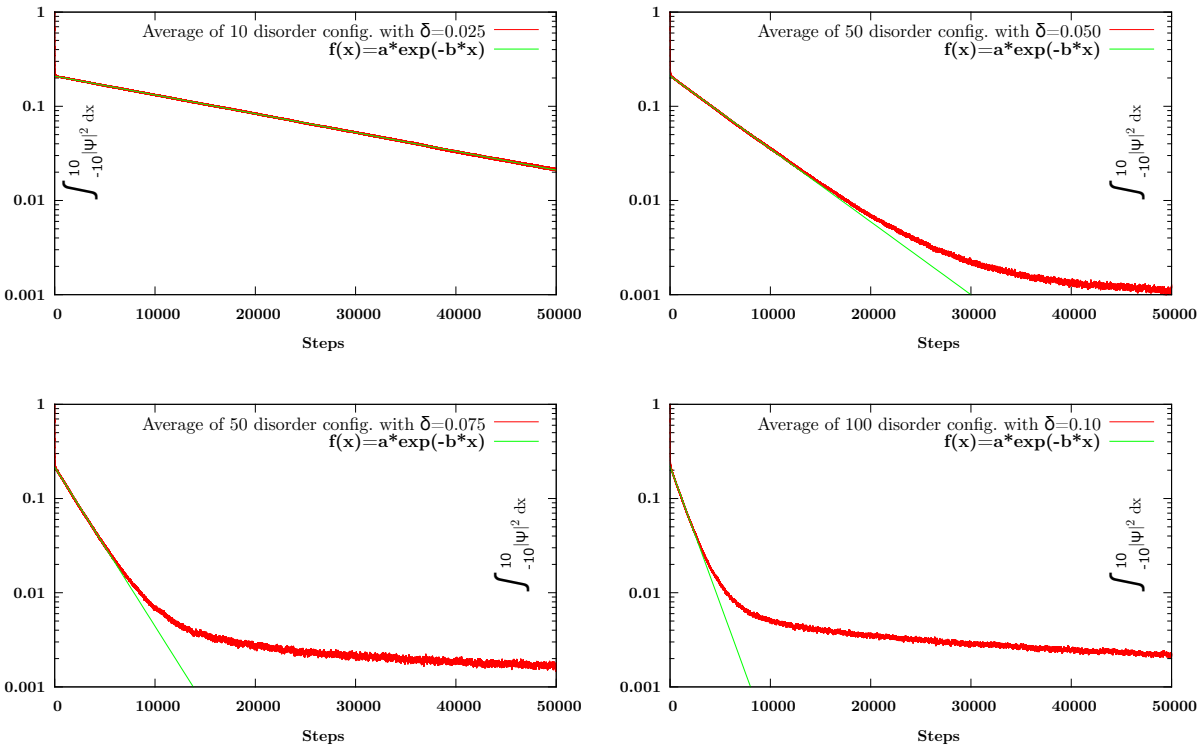

Figure 5.5.: Integrated weight of the wave-function around the spatial boundary of topologically distinct phases at $x = 0$ for the STQW under the effect of dynamic disorder. The disorder parameters are chosen as follows: $\delta = 0.025, 0.05, 0.75, 0.10$. One can observe that the bound states only decay exponentially in a limited region. At some point, depending on the strength of the disorder δ, the behaviour of the bound state is governed by diffusion processes. These are referred to as 'diffusive tails'.

After fitting the decay curves in the appropriate region for various strength of disorder, one can plot the time constants b against the disorder parameter δ. One observes that the time constants scale quadratically with δ, for small disorder parameter. For stronger disorder, the bound states decay rapidly, and the dynamics of the system is governed by diffusion rather than by an exponential decay.

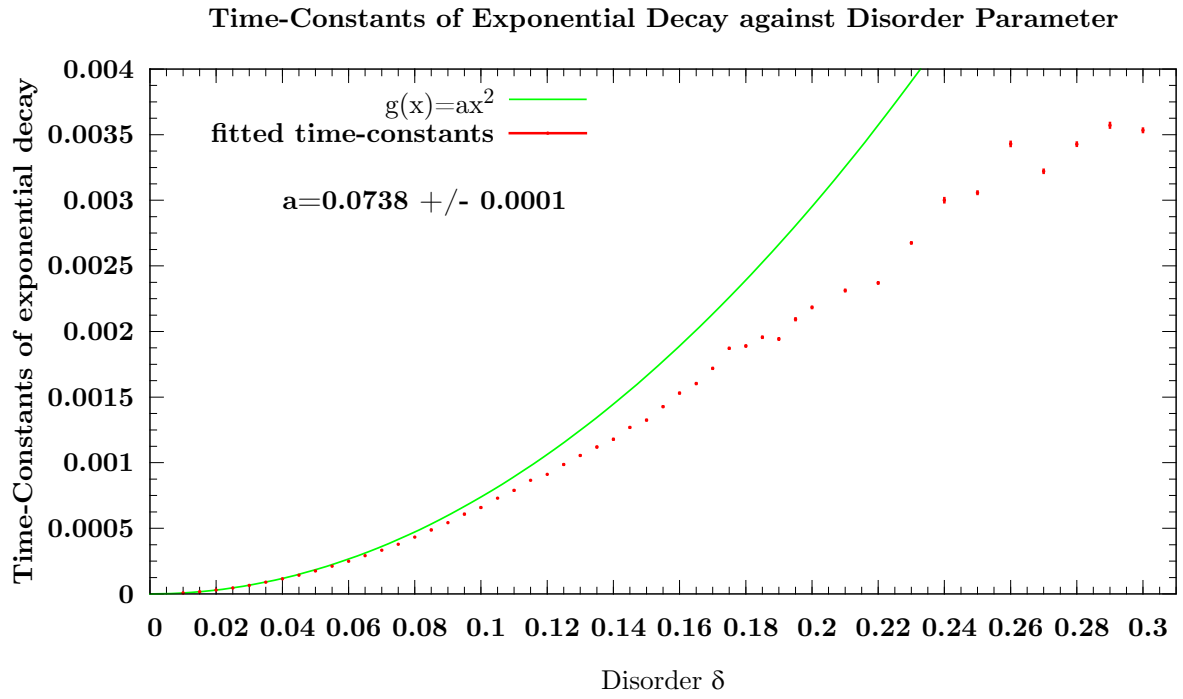

Figure 5.6.: Extracted time constants of the exponential decay of the bound states that are subject to dynamic disorder.
For weak perturbations, the time constants of the exponential decay scale quadratically with the disorder parameter.
In case of strong-disorder, deviations from the fitted curve ($g(x) = ax^2$) become visible. This is because the behaviour of the bound state is described by the laws of diffusion rather than by an exponential decay.

For small disorder parameters the following equation for the time constants is obtained numerically:

$$g(\delta) = a\delta^2 \quad \text{with } a = (0.0738 \pm 0.0001) \tag{5.4}$$

A list of all time constants can be found in table A.2.

5.3. Dynamic Disorder (Correlation Lengths)

In the previous section, the perturbation configuration of the system changed at every iteration of the split-step protocol. Therefore, every time a part of the wave function is set free due to disorder, it can get recaptured in the next iteration of the STQW that realises a different disorder configuration. This problem can be tackled by introducing a spatial (ξ) and a temporal (w) correlation length for the system. After each change of the disorder configuration, the disorder is kept unchanged for w iterations of the STQW protocol. The spatial correlation length blurs the area, where the bound state is localized if $\theta_2(x,t)$ depends on ξ, with:

$$\theta_2(x,\xi,t) = \frac{1}{2}(\theta_{2-} + \theta_{2+}) + \frac{1}{2}(\theta_{2+} - \theta_{2-}) \tanh\left(\frac{x}{\xi}\right) + \delta\gamma(x,t) \tag{5.5}$$

$$\theta_2(x,\xi,t) = \begin{cases} \theta_{2-} + \delta\gamma(x,t), & x \gg 0 \\ \theta_{2+} + \delta\gamma(x,t), & x \ll 0 \end{cases} \tag{5.6}$$

The asymptotic limit of the function, however, remains unchanged.

The decay curves are fitted for their effective step lengths only, meaning that only those steps are considered, where the disorder actually changes (after every w-th step). Hence, one has to calculate the decay coefficients for a larger set of parameters (w, ξ, δ).

$$\begin{aligned} \delta &\in [0.01, \ldots, 0.2] \\ w &\in [50, 75, 100] \\ \xi &\in [1.5, 3, 4.5, 6] \end{aligned}$$

This procedure is of particular importance because it allows comparison with the analytical calculation for the decay coefficients done in the following chapter. Again, the fitting for the exponential decay (fit-function $f(x) = ae^{-bx}$) is limited to a specific region (depending on the strength of the disorder δ and the waiting time w) because of the appearance of diffusive tails, similar to those in Fig. 5.5. The time constants b are listed in Table 5.2.

Time constants of the exponential decay with correlation lengths w and ξ

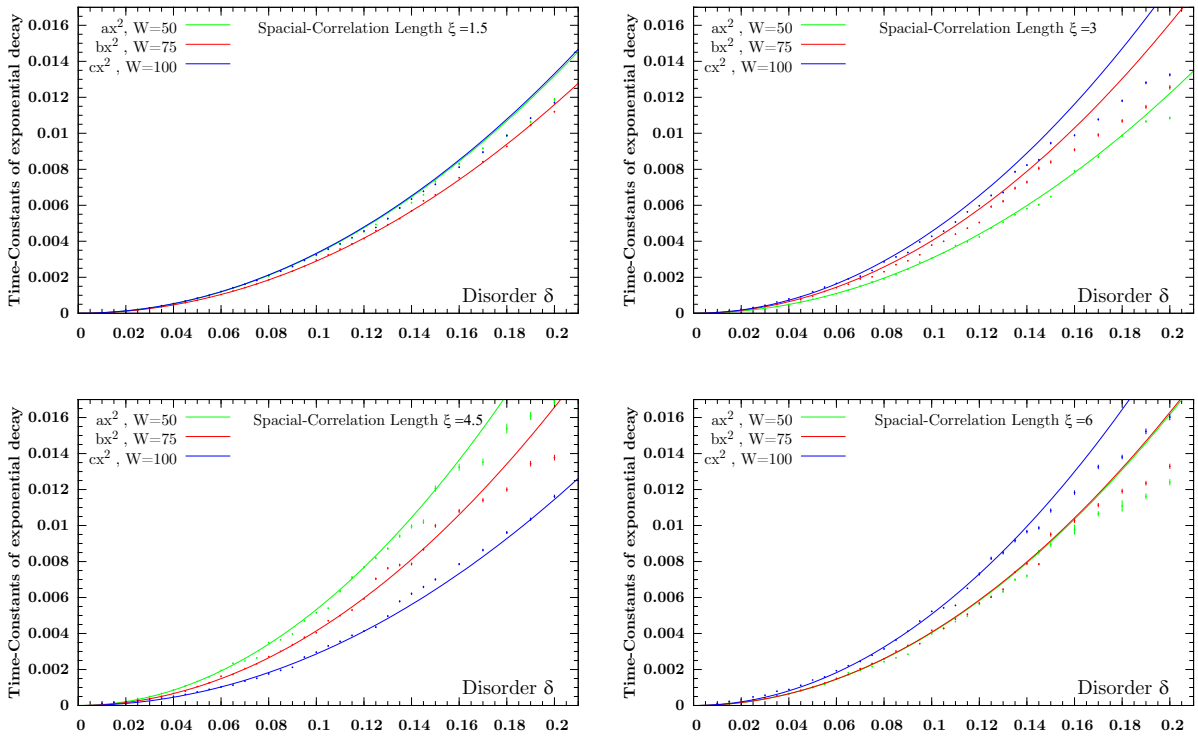

Figure 5.7.: Time constants of the exponential decay with correlation lengths w and ξ. One can see that the decay constants of the bound states scale quadratically with the disorder parameters for small disorder strengths. For greater disorder parameters, deviations from the quadratic curvature become visible. A list of all fit-values can be found in Tables A.4, A.5, A.6

5.4. Diffusive Tails

In case of time-dependent disorder, the motion of the wave function (in the long-term, after the bound states decayed) is described by the laws of diffusion. This is not the case for static disorder. The diffusion equation for the system is:

$$\frac{\partial}{\partial t} n(x,t) = D \frac{\partial^2}{\partial x^2} n(x,t) \tag{5.7}$$

$$n(x,t) = \frac{1}{2\sqrt{\pi D t}} \exp\left(\frac{-x^2}{4Dt}\right) \tag{5.8}$$

w	ξ	b	Δb
50		0.330	0.001
75	1.5	0.290	0.001
100		0.333	0.001
1		0.0738	0.0001
50		0.305	0.004
75	3	0.402	0.014
100		0.454	0.009
50		0.533	0.005
75	4.5	0.414	0.003
100		0.286	0.006
50		0.404	0.008
75	6	0.407	0.005
100		0.508	0.008

Table 5.2.: Time constants of the exponential decay for various ξ and w.

$n(x,t)$ is the probability-density and takes the form of a Gaussian distribution, with a width $\Delta x \propto \sqrt{Dt}$, where D is the diffusion coefficient.

In the long-time limit ($t \to \infty$), the probability-density n decays slowly with $n \propto \frac{\delta}{\sqrt{t}}$ at the origin.

$$\lim_{t\to\infty} \int_{-a}^{a} \left(\frac{n(x,t)}{1/\sqrt{t}} \right) dx = \lim_{t\to\infty} \left(\operatorname{erf}\left(\frac{a}{2\sqrt{Dt}} \right) \sqrt{t} \right) = \frac{a}{\sqrt{\pi}\sqrt{D}} = 5.6419 \frac{1}{\sqrt{D}} \propto 5.6419 \cdot \delta \tag{5.9}$$

, where the diffusion coefficient D scales with the disorder parameter δ as $\frac{1}{\sqrt{D}} \propto \delta$ $\left(D = \left\langle v_{Drift}^2 \tau \right\rangle \propto \frac{1}{\delta^2}, \text{ Fermi's Golden Rule} \right)$. Here, a is chosen to be 10. The proportionality constant can be calculated numerically by an investigation of the long-term behaviour of the probability-density by fitting the diffusive tails with respect to $A(\delta)$ and B for a range of large disorder parameters ($\delta \in [0.07, 0.30]$). The fitting function is chosen as:

$$n_\delta(t) = A(\delta) \frac{1}{t^B} \tag{5.10}$$

In a plot with a double logarithmic-scale this takes the form of a linear equation:

$$\log(n_\delta(t)) = \log\left(A(\delta)\right) - B \cdot t \tag{5.11}$$

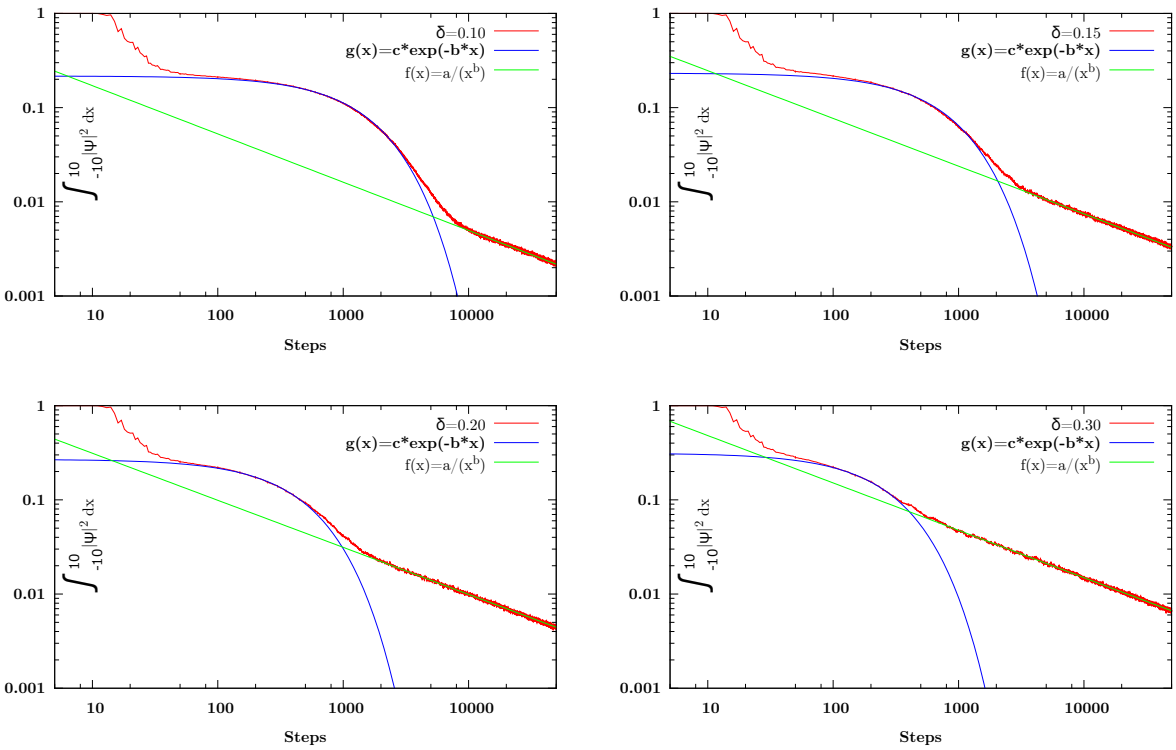

Figure 5.8.: In a double-logarithmic scale the long term behaviour of the density, which describes the diffusive tails mathematically, is of the form $n_\delta(t) = A(\delta) - Bt$. These coefficients are found through numeric fit for various disorder parameters.
With increasing strength of the disorder δ, the crossover region between the exponential decay and the diffusive tails becomes smaller.

The numerical evaluation of the coefficient A(δ) can be seen in Fig. 5.9. The fit-parameters for each disorder-parameter δ can be found in Table A.1.

	Theory	Numerical Calculation
$A(\delta)$		5.06 ± 0.03
B	0.5	0.503± 0.001

Table 5.3.: Theoretical predictions and numerical calculations for the exponent B

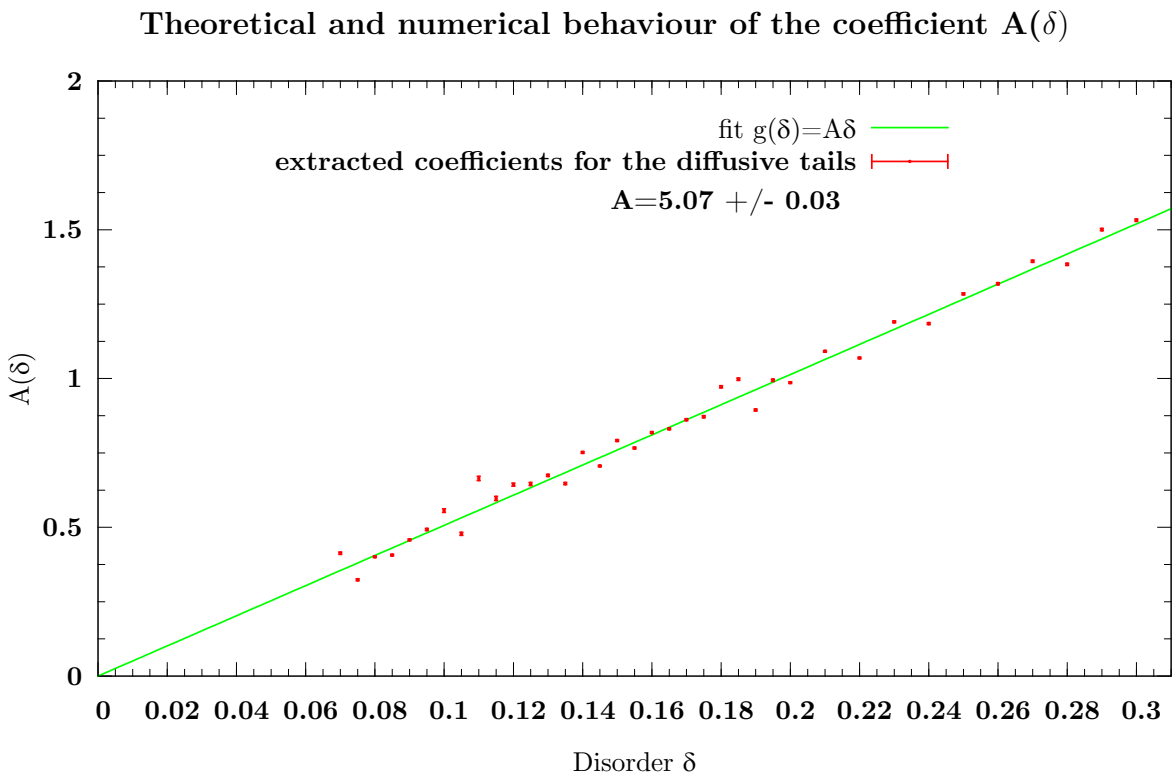

Figure 5.9.: Numerical results for the coefficient A(δ) in the long-term behaviour of the density $n_\delta(x,t)$.

Therefore, the proportionality constant α, $\left(\frac{1}{\sqrt{D}} = \alpha\delta\right)$ is numerically determined to be:

$$\alpha = 0.897 \pm 0.005 \tag{5.12}$$

5.5. Analytical Investigation of the Decay for the Bound State

5.5.1. Calculation of the Bound State – The Bulk Hamiltonian

In order to find an analytical solution for the time-constants of the exponential decay of the bound states that are subject to dynamic disorder one can calculate a bulk Hamiltonian $\mathcal{H}_{bulk}$ out of the STQW by a series expansion around the phase-transition point, *i.e.* $k = 0$, $\theta_2 = \pi/2$.

$$\vec{n}_{bulk} = \lim_{\theta_1 \to -\pi/2} \left(\sum_{n \geq 0} \frac{\partial^n}{\partial \theta_2^n n!} \left(\sum_{l \geq 0} \frac{\partial^l}{\partial k^l l!} \vec{n}(0, \theta_1, \pi/2) k^l \right) (\theta_2 - \pi/2)^n \right) \tag{5.13}$$

$$n_x(k, -\frac{\pi}{2}, \theta_2) = -\frac{1}{2}k - \frac{1}{8}(\pi - 2\theta_2) + O(k^2, \theta_2^2) \tag{5.14}$$

$$n_y(k, -\frac{\pi}{2}, \theta_2) = -\frac{\pi}{4} + \frac{\theta_2}{2} + O(k^2, \theta_2^2) \tag{5.15}$$

$$n_z(k, -\frac{\pi}{2}, \theta_2) = -\frac{1}{2}k - \frac{1}{8}(\pi - 2\theta_2) + O(k^2, \theta_2^2) \tag{5.16}$$

The weak-dependence of n_x, n_z on θ_2 is neglected by setting $\theta_2 = \frac{\pi}{2}$. The wave function for the bound state at $x = 0$ with energy $E = 0$ is obtained by solving the eigenvalue equation $\mathcal{H}_{bulk}\Psi(x) = E\Psi(x)$ that takes the form of a Dirac equation (boxed).

$$\mathcal{H}_{bulk}\Psi(x) = \vec{n}_{bulk} \cdot \vec{\sigma} = E\Psi(x) \stackrel{!}{=} 0 \tag{5.17}$$

$$\boxed{\left(\frac{i}{2}\partial_x(\sigma_x + \sigma_z) + \left(\frac{\theta_2}{2} - \frac{\pi}{4} \right) \sigma_y \right) \Psi(x) = 0} \tag{5.18}$$

$$\left(\partial_x \mathbb{1} + \mathbb{M} \frac{(-m(x))}{2} \right) \Psi(x) = 0 \tag{5.19}$$

$$\text{with} \quad \mathbb{M} = -i2 \cdot (\sigma_x + \sigma_z)^{-1} \sigma_y = \begin{pmatrix} 1 & -1 \\ -1 & -1 \end{pmatrix} \tag{5.20}$$

$$m(x) \equiv \left(\frac{\pi}{2} - \theta_2(x) \right) \tag{5.21}$$

After making the ansatz $\vec{\psi}(x) = \vec{a}e^{\lambda(x)}$ we obtain the eigenvalue equation:

$$\mathbb{M}\vec{a} = \left(\frac{2}{m(x)} \frac{\partial}{\partial x} \lambda(x) \right) \equiv \gamma \vec{a} \tag{5.22}$$

The eigenvalues and eigenvectors of $\mathbb{M}$ are:

$$\vec{a}_- = \begin{pmatrix} \sqrt{2}-1 \\ 1 \end{pmatrix} \qquad \vec{a}_+ = \begin{pmatrix} -\sqrt{2}-1 \\ 1 \end{pmatrix} \tag{5.23}$$

$$\gamma_- = -\sqrt{2} \qquad \gamma_+ = \sqrt{2} \tag{5.24}$$

Solving Eq. (5.22) for $\lambda(x)$ one obtains

$$\lambda(x)_\pm = \pm\frac{1}{\sqrt{2}}\int_0^x m(x)dx + \lambda(0) \tag{5.25}$$

The general solution is:

$$\vec{\Psi}(x) = \vec{a}_- e^{\lambda_+(x)} + \vec{a}_+ e^{\lambda_-(x)} \tag{5.26}$$

$$\text{with} \quad \frac{\pi}{2} - \theta_2(x) = \frac{\pi}{4}\tanh(\frac{x}{3}) = m(x) \begin{cases} > 0, & x > 0 \\ 0, & x = 0 \\ < 0, & x < 0 \end{cases} \tag{5.27}$$

Due to the normalisation condition of the wave function, $\lim\limits_{x\to\pm\infty} |\psi(x)|^2 < \infty$, $\lambda(x)_+$ is no solution. The solution for the wave function therefore is:

$$\vec{\psi}(x) = \psi_0 \begin{pmatrix} \sqrt{2}-1 \\ 1 \end{pmatrix} e^{-\frac{1}{\sqrt{2}}\int_0^x m(x)dx} = \frac{1}{5.197023}\begin{pmatrix} \sqrt{2}-1 \\ 1 \end{pmatrix} \cosh\left(\frac{x}{3}\right)^{-\frac{3\pi}{4\sqrt{2}}} \tag{5.28}$$

where $\lambda(0) \equiv \psi_0 = \frac{1}{\sqrt{5.197023}}$ has been evaluated numerically.
The plot of $|\vec{\Psi}|^2 = 0.225432\cosh(\frac{x}{3})^{\frac{-3\pi}{2\sqrt{2}}}$ can be seen in Fig. 5.10. In Fig. 5.12 it is shown that the agreement gets better if $\theta_{2\pm}$ is chosen closer to $\frac{\pi}{2}$.

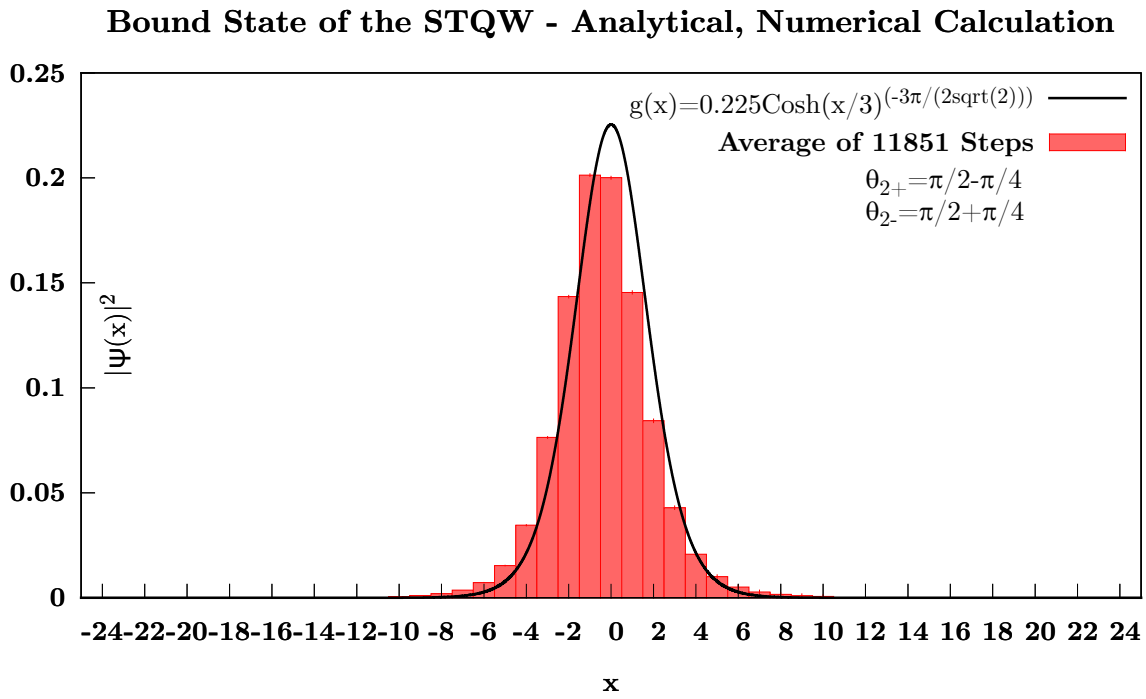

Figure 5.10.: The bound state of the STQW obtained from the solution of Eq. (5.18). The **red boxes** represent the average of the Bound State for 11851 iterations of the STQW-Protocol, error bars included. The averaging started after iteration 59. The continuum solution is plotted as a **black line**. The analytical solution is axisymmetrical to the y-axis whereas the numerically obtained solution seems to be shifted to the left. However, the full width at half maximum and the sharp decline of the analytical and numerical solution coincide.

5.5.2. Calculation of the Decay Coefficients

The simplest way to obtain an analytical expression for the decay coefficients of the bound states is to consider the overlap of two disturbed wave functions. For a fixed disorder realization, the expression for the overlap becomes:

$$\begin{aligned}
\frac{\langle\Psi_i|\Psi_{i+1}\rangle}{\sqrt{\langle\Psi_i|\Psi_i\rangle\,\langle\Psi_{i+1}|\Psi_{i+1}\rangle}} &\overset{(5.33)}{=} \frac{\int_{-\infty}^{\infty} f(x)\exp\left(-1/\sqrt{2}\int_0^x \left(\delta_i(x'')+\delta_{i+1}(x'')\right)dx''\right)dx}{\int_{-\infty}^{\infty} f(x)\exp\left(\frac{-2}{\sqrt{2}}\int_0^x \delta_i(x')dx'\right)dx \int_{-\infty}^{\infty} f(x''')\exp\left(\frac{-2}{\sqrt{2}}\int_0^{x'''} \delta_{i+1}(x'')dx''\right)dx'''} \\
&\overset{(5.34)}{\approx} \frac{1-1/\sqrt{2}\left(\langle\Delta_i\rangle+\langle\Delta_{i+1}\rangle\right)+1/4\,\langle(\Delta_i+\Delta_{i+1})\rangle}{\sqrt{1-\sqrt{2}\left(\langle\Delta_i\rangle+\langle\Delta_{i+1}\rangle\right)+2\,\langle\Delta_i\rangle\,\langle\Delta_{i+1}\rangle+\langle\Delta_i^2\rangle+\langle\Delta_{i+1}^2\rangle}} \\
&\overset{(5.35)}{\approx} 1+\frac{1}{4}\left(\langle\Delta_i\rangle^2-\left\langle\Delta_i^2\right\rangle+\langle\Delta_{i+1}\rangle^2-\left\langle\Delta_{i+1}^2\right\rangle\right) \qquad (5.29) \\
&\quad +\frac{1}{2}\left(\langle\Delta_i\Delta_{i+1}\rangle-\langle\Delta_i\rangle\,\langle\Delta_{i+1}\rangle\right) \\
&= 1-\frac{1}{4}\left(\left\langle(\Delta_i-\Delta_{i+1})^2\right\rangle-\langle(\Delta_i-\Delta_{i+1})\rangle^2\right) \qquad (5.30)
\end{aligned}$$

Now, we average over disorder realizations to obtain:

$$\begin{aligned}
\overline{\left\langle\frac{\langle\Psi_i|\Psi_{i+1}\rangle}{\sqrt{\langle\Psi_i|\Psi_i\rangle\,\langle\Psi_{i+1}|\Psi_{i+1}\rangle}}\right\rangle} &= 1+\frac{1}{2}\delta^2\left(\langle x\rangle\,\langle\mathrm{sgn}(x)\rangle-\langle|x|\rangle\right) \\
&\overset{(5.36)}{=} 1-\frac{1}{2}\delta^2\,\langle|x|\rangle = 1-\frac{1}{6}\delta_i^2\,\langle|x|\rangle \\
&\approx \exp\left(-\frac{1}{6}\delta_i^2\,\langle|x|\rangle\right)
\end{aligned}$$

Based on the assumption that there are no other excited states left after a change in disorder, the analytical solution for the decay of the bound-states after N steps is:

$$\left(\overline{\left\langle\frac{\langle\Psi_i|\Psi_{i+1}\rangle}{\sqrt{\langle\Psi_i|\Psi_i\rangle\,\langle\Psi_{i+1}|\Psi_{i+1}\rangle}}\right\rangle}\right)^N \approx \exp\left(-N\frac{1}{6}\delta_i^2\,\langle|x|\rangle\right) \qquad (5.31)$$

$\langle|x|\rangle$ can be understood as the correlation length of the system, because it depends on the particular choice of the width of the $\theta_{2w}(x,\xi,t)$ function blurring the area where the bound state is localized.

$$\langle|x|\rangle = \frac{\sum_{x=-a}^{a}|x|f(x)}{\sum_{x=-a}^{a}f(x)} = \frac{\sum_{x=-a}^{b}|x|\psi_0^2\vec{a}_-^2\cosh\left(\frac{x}{w}\right)^{-\frac{2w\pi}{4\sqrt{2}}}}{\sum_{x=-a}^{a}\psi_0^2\vec{a}_-^2\frac{2w\pi}{4\sqrt{2}}\cosh\left(\frac{x}{w}\right)^{-\frac{2w\pi}{4\sqrt{2}}}} \tag{5.32}$$

The area of integration (choice of a) depends on the choice of w.

In this calculation, all terms of third order have been omitted. If Δ_i and Δ_{i+1} happen to be the same disorder configuration, the overlap $\langle\Psi_i|\Psi_{i+1}\rangle$ is 1, see Eq. (5.30). This is equivalent to the stationary disorder configuration, where the energy of the system is conserved. Consequently, the numerical calculations from section 5.1 match with the analytical calculations.

In the calculation of the overlap, the following abbreviations have been used.

$$f(x) = \psi_0^2\vec{a}_-^2 \cdot \exp\left(\frac{-2}{\sqrt{2}}\int_0^x m(x')dx'\right) \tag{5.33}$$

$$\Delta_i(x) \equiv \int_0^x \delta_i(x)dx, \quad \exp(x) = 1 + x + \frac{1}{2}x^2 + O(x^3), \quad \langle g(x)\rangle \equiv \frac{\int_{-\infty}^{\infty} f(x)g(x)dx}{\int_{-\infty}^{\infty} f(x)dx} \tag{5.34}$$

$$\frac{1}{\sqrt{1+x}} = 1 - \frac{1}{2}x + \frac{3}{8}x^2 + O(x^3) \tag{5.35}$$

Here, the Δ- terms can be evaluated in the following sense:

$$\left\langle \Delta_i^2 \right\rangle = \left\langle \int_0^x dx' \int_0^x dx'' \delta_i(x')\delta_i(x'') \right\rangle \overset{5.37}{=} \frac{1}{3}\delta_i^2 \left\langle \int_0^x \int_0^x \delta(x'-x'')dx'dx'' \right\rangle \overset{5.38}{=} \frac{1}{3}\delta_i^2 \left\langle |x| \right\rangle \quad (5.36)$$

$$\left\langle \delta_i(x')\delta_i(x'') \right\rangle_{Dis} \equiv \delta^2\delta_{distr}(x'-x'') = \frac{\int_{-\delta_i}^{\delta_i} \delta_i^{2\prime} d\delta_i'}{\int_{-\delta_i}^{\delta_i} d\delta_i'} \delta(x'-x'') = \frac{1}{3}\delta_i^2\delta(x'-x'') \quad (5.37)$$

$$\int_0^x \delta(x'-x'')dx' = \begin{cases} 1 & : x > 0 \quad \wedge \quad x'' \in (0,x) \\ -1 & : x < 0 \quad \wedge \quad x'' \in (0,x) \end{cases} \quad (5.38)$$

After a similar procedure one obtains $\left\langle \Delta_i \right\rangle^2 = \frac{1}{3}\delta_i^2 \left\langle x \right\rangle \left\langle \mathrm{sgn}(x) \right\rangle$
, where the terms $\left\langle \Delta_i\Delta_{i+1} \right\rangle, \left\langle \Delta_i \right\rangle \left\langle \Delta_{i+1} \right\rangle$ reduce to 0, because the disorder average of $\left\langle \Delta_i\Delta_{i+1} \right\rangle_{Dis}$ is zero.

w	ξ	b	Δb	Theory
50		0.330	0.001	
75	1.5	0.290	0.001	0.185
100		0.333	0.001	
1		0.0738	0.0001	
50		0.305	0.004	
75	3	0.402	0.014	0.241
100		0.454	0.009	
50		0.533	0.005	
75	4.5	0.414	0.003	0.286
100		0.286	0.006	
50		0.404	0.008	
75	6	0.407	0.005	0.325
100		0.508	0.008	

Table 5.4.: Comparing time-constants of the exponential decay of the bound-states

5.6. Comparing Numerical Results with Theoretical Expectations

The analytical decay constants for the bound state $\left(-\frac{1}{6}\delta_i^2 \langle|x|\rangle\right)$ have been evaluated using Eq. (5.32) with the appropriate expressions for w. ξ determined the area of integration (see section 5.3). These numerically obtained prefactors, denoted b in Table 5.4, are the fit constants from Eq. $(f(\delta_i) = b\delta_i^2)$, see Fig. 5.7.

Observation - Numerical Calculation

First, one observes that the numerically calculated values for b, do not scale appropriately within each value for ξ. The expectation is that the decay factors b for each value of the disorder change w remain unchanged. In all cases, ξ has been chosen much smaller than the disorder change ($\xi \ll w$), with the intention that parts of the wave function, released by a change in disorder (including excited states), move out of the area of integration, preventing a recapture in the bound state.

Interpretation - Numerical Results

The discrepancy between the decay factors b within each region of ξ is not caused by a finite size effect of the system (as discussed in section 6.1). The size of the system scaled with the number of iterations of the split-step protocol, in order to avert boundary effects. Furthermore, it could be observed that the decay of the bound states for the first

effective steps (where 'first' depends on the choice of ξ) is not exponential, in contrast to assumptions, which is one reason for the deviations of the values for b for a fixed ξ. This can be seen exemplary in Fig. 5.11. What is more, it has been shown in section 5.1 that static disorder in one dimension leads to conservation of energy, meaning that the wave function remains localized. In consequence, the assumption that has been made in section 5.3 proved to be wrong. It was assumed that parts of the wave function, that are set free due to a disorder change, can be effectively transported out of the bound state, if the disorder-configuration is kept unchanged for w steps. The behaviour of the bound state was then investigated for an effective step length (every w-th-step). This was done in order to be able to compare the numerical results with analytical calculations.

One suggestion for future investigations of the decay of the bound states is, to remove any kind of disorder outside the bound state completely, so that during the waiting time w the disorder is kept unchanged only inside the bound state.

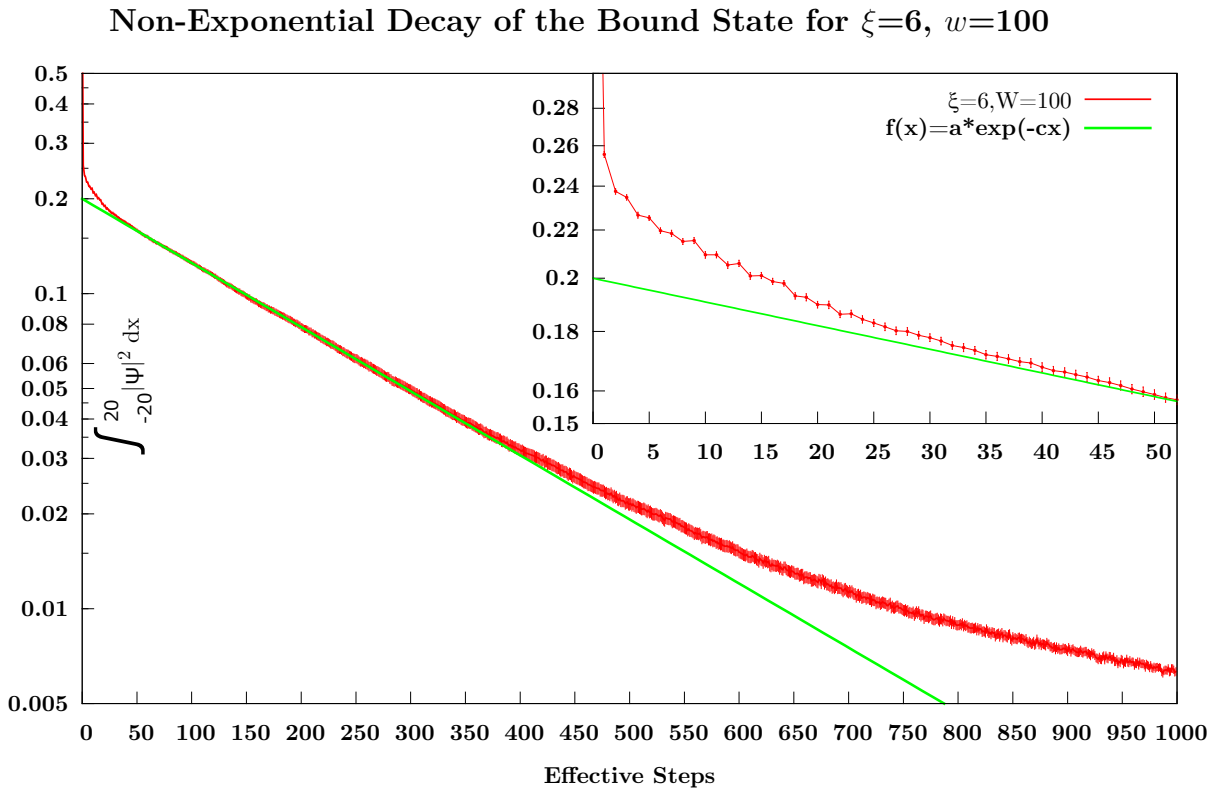

Figure 5.11.: It can be observed, that for the first effective steps, the decay of the bound state is not exponential, in contrast to assumptions.

Analytical Procedure

During the analytical calculation for the wave function of the bound state, the assumption was made that $\theta_2(x,t,\xi)$ is always close to the value of $\frac{\pi}{2}$ in order to neglect the weak dependence of n_x (Eq. (5.14)) and n_z (Eq. (5.16)) on θ_2. This is only true in the vicinity of the gap closing point as:

$$\theta_2(x) = \begin{cases} \frac{\pi}{2} + \frac{\pi}{4}, & x \gg 0 \\ \frac{\pi}{2} - \frac{\pi}{4}, & x \ll 0 \end{cases}$$

However, the numerical calculations for the bound state are in good accordance with the theoretically obtained wave function, see Fig. 5.10. Nevertheless, it is suggested to chose $\theta_2\pm$ close to $\frac{\pi}{2}$ as in Fig. 5.12. It can be observed that the numerically and analytically obtained solution for the wave function of the bound state are in good accordance. The constant shift between the continuum solution and the numerical solution for all $\theta_{2\pm}$ is just an effect of the box-distribution of the numerical solution on integer lattice sites.

Comparing Numerics with Theoretical Predictions for different $\theta_{2\pm}$

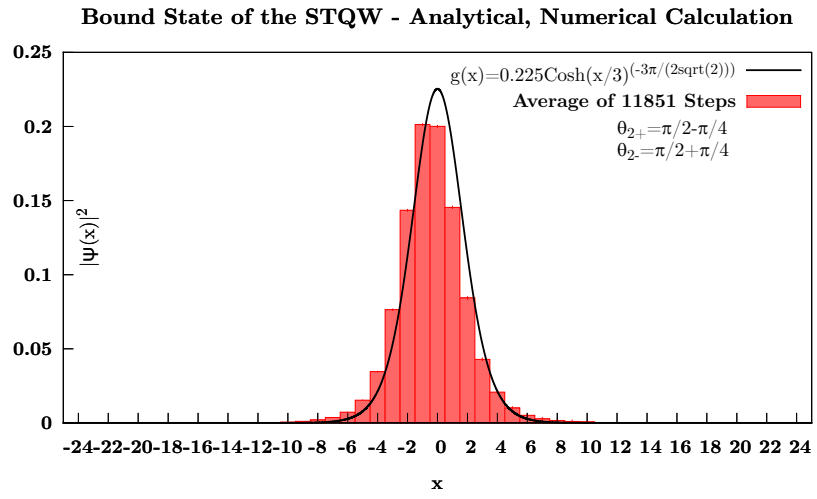

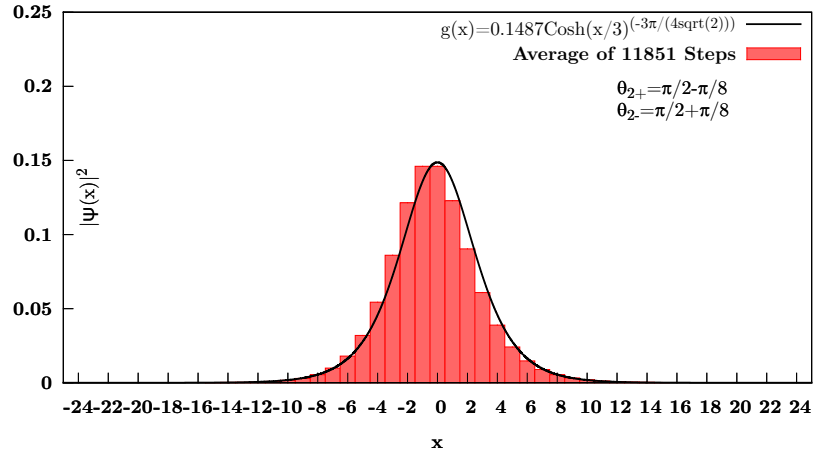

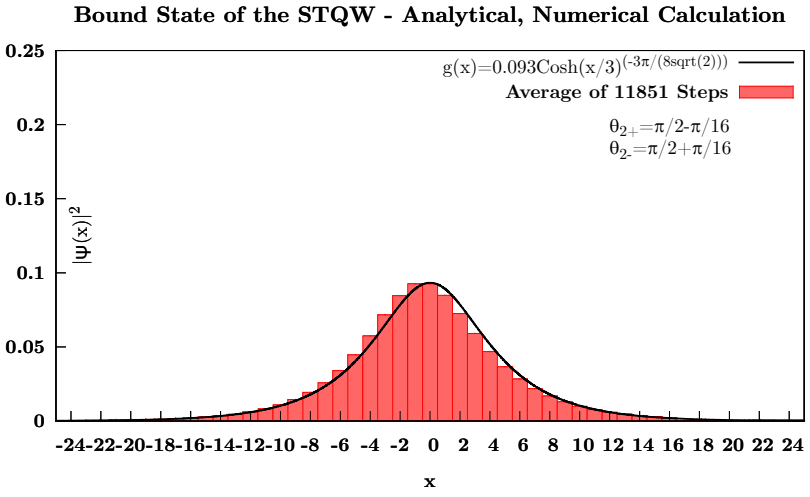

Figure 5.12.: Numerical and analytical solution of the bound state for $\theta_{2\pm}$ close to $\frac{\pi}{2}$

6. Programming the Quantum Walk

6.1. Improving the Runtime - Finite Size Effect

The Split-Step Quantum Walk (STQW) was programmed in `C/C++`. Its runtime is quadratic in the number of steps:

$$\sum_{n=0}^{N}(2n+1) \in O(N^2) \tag{6.1}$$

The reason is, that the number of steps scales with the size of the system. With each iteration of the split step protocol the range of the walker can expand by one lattice site in each direction. For N steps of the STQW-protocol one has to allocate memory for a system that contains at least $2N + 1$ slots.

For small disorder parameters it is necessary to iterate the split step-protocol many times ($N \approx 10^5$). The larger the disorder parameter, the less steps are needed to destroy the bound state. At the same time, the number of disorder configurations has to be increased to suppress the fluctuations in the decay curves.

As the focus lies on the behaviour of the bound state, the observation of a limited region from $x = -10$ to $x = 10$ is sufficient. Therefore, the size of the system can be reduced to improve the program's runtime. This was implemented by using open boundary conditions. The influence on the bound state was investigated by comparing the results of a system with normal size $(2N + 1)$ to a system with a size reduced by a factor of 10 by plotting the difference of the probability of presence around the localized state. The results can be seen in Fig. 6.1.

Apparently, while some part of the wave function vanishes as it reaches the boundary of the system, the other part behaves as if it were reflected by a high potential. This can be seen in Fig. 6.2. If the disorder parameter is non-zero, the effects on the difference in the probability of presence from the bound state are worse.

The idea to reduce the size of the system to improve the runtime was cast away. It might have been possible to implement a function in the region of the boundary that would exponentially suppress the rate of reflection by slowly increasing the rate of elimination $\propto \exp(-(x - x_0))$. The correct adjustment of the function would have been complicated.

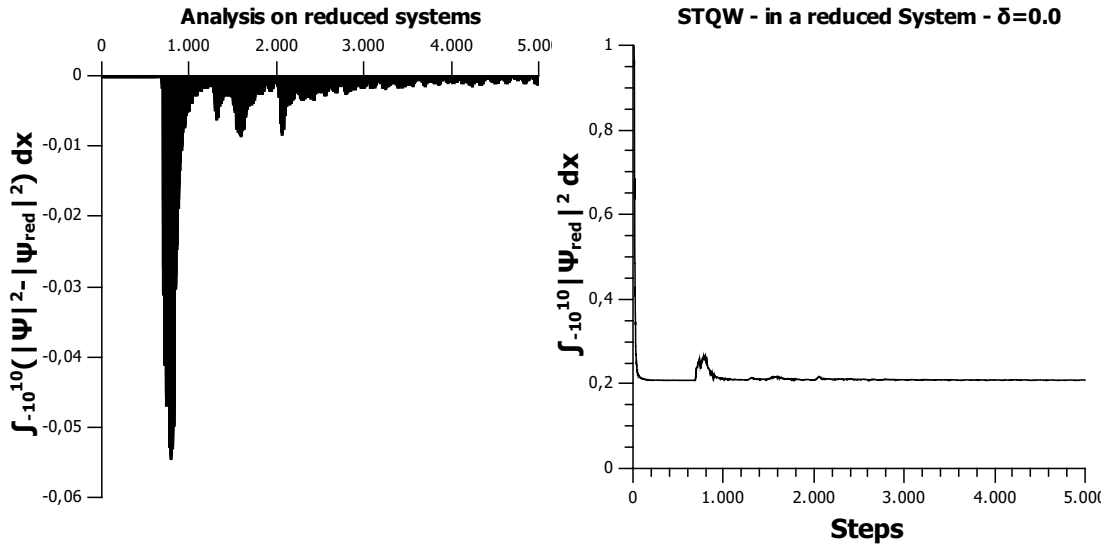

Figure 6.1.: **Left:** On the y-axis there is the difference of the weight of the bound state between a wave-function with normal- and reduced system size. On the x-axis there is the number of iterations of the STQW (Eq. 4.4).
Right: A part of the wave function of the system was reflected at the system's boundary and travelled back to the localised state.

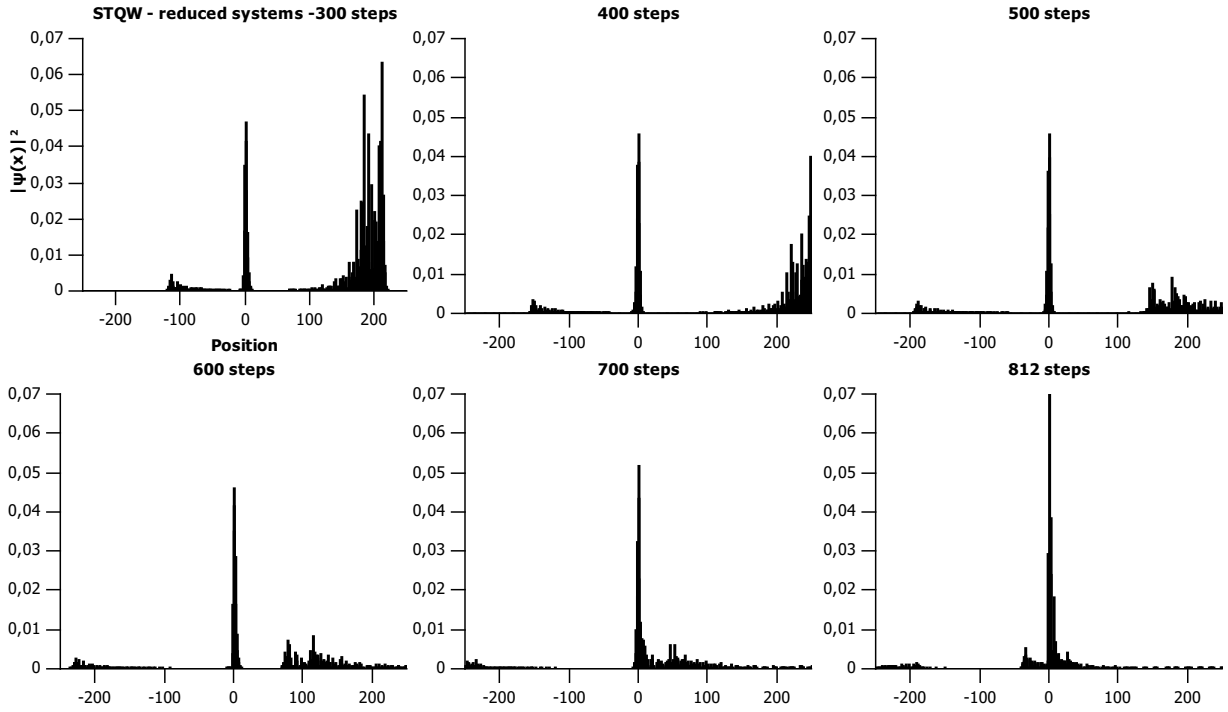

Figure 6.2.: Probability distribution of the split step quantum walk plotted for different numbers of steps in a reduced system with open boundary conditions. It can be observed that a part of the wave packet is reflected at the boundary of the system and further traverses in the opposite direction, finally returning to the localised state.

7. Outlook - Quantum Walk on a Square Lattice (2D)

Kitagawa, Rudner, Berg, and Demler showed, in analogy to the 1D split-step protocol, that it is possible to manipulate the discrete-time-quantum walk in two dimensions in a way that allows it to support distinct topological phases [1].

In their paper [1], they discussed the 2D quantum walk on a triangular lattice and suggested an equivalent implementation on a square lattice as it might be easier to realize in an experimental setting (e.g. cold atoms in optical lattices). It is then of particular importance to know about the effects of time-dependent disorder (that occur in an experiment) on the time-evolution of the system. Therefore one of the aims for future calculation (both numerically and analytically) is the investigation of disordered systems in two dimensions with both static and dynamic disorder.

The 2D quantum walk is determined by the sequence of unitary transformations:

$$\boldsymbol{U_{2D,ss}} = \boldsymbol{T_{3,\uparrow,\downarrow}} \boldsymbol{R}(\theta_1) \boldsymbol{T_{2,\uparrow,\downarrow}} \boldsymbol{R}(\theta_2) \boldsymbol{T_{1,\uparrow,\downarrow}} \boldsymbol{R}(\theta_1) \tag{7.1}$$

$\boldsymbol{T_{i,\uparrow,\downarrow}}$ is a spin-dependent delocalisation of the particle that shifts spin-up (spin-down) components in the direction of +(-) $\vec{w}_i$ (see Fig. 7.1).

Translation-Vectors for the 2D Quantum Walk on a Square Lattice

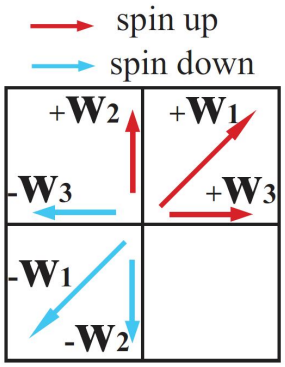

Figure 7.1.: Translation vectors $\vec{w}_1 = (1, 1)$ $\vec{w}_2 = (0, 1)$ and $\vec{w}_3 = (1, 0)$. Figure taken from [1]

The Hamiltonian of the system is of the same form as the Hamiltonian for the STQW in 1D, see Eq. (4.6).

$$\boldsymbol{\mathcal{H}_{2D,ss}} = \iint_{BZ} dk_x dk_y \quad E_{\theta_1,\theta_2}(k_x,k_y)\vec{n}(\theta_1,\theta_2,k_x,k_y) \cdot \sigma \times |kx,ky\rangle \langle kx,ky| \tag{7.2}$$

$$\boldsymbol{U_{2D,ss}} = \exp\left(-i\boldsymbol{\mathcal{H}_{2D,ss}}\right) \qquad ,\hbar = 1 \tag{7.3}$$

The relation between $\boldsymbol{U_{2D,ss}}$ and $\boldsymbol{\mathcal{H}_{2D,ss}}$ can be derived similarly to the 1D case. Therefore, one obtains the following set of equations for the energy E and the unit vector $\vec{n}$:

$$\begin{aligned}\cos\left(E_{\theta_1,\theta_2}(k_x,k_y)\right) =& \cos\left(\theta_2/2\right)\left(\cos(k_x)\cos(k_x+2k_y)\cos(\theta_1) - \sin(k_x)\sin(k_x+2k_y)\right)\\ &- \cos^2(k_x)\sin(\theta_1)\sin(\theta_2/2)\end{aligned}$$

$$\begin{aligned}\sin\left(E_{\theta_1,\theta_2}(k_x,k_y)\right) n_x(\theta_1,\theta_2,k_x,k_y) &= \cos(k_x+2k_y)\cos\left(\theta_2/2\right)\sin(k_x)\sin(\theta_1)\\ &\quad - \sin(2k_x)\sin^2\left(\theta_1/2\right)\sin\left(\theta_2/2\right)\\ \sin\left(E_{\theta_1,\theta_2}(k_x,k_y)\right) n_y(\theta_1,\theta_2,k_x,k_y) &= \cos(k_x)\cos(k_x+2k_y)\cos\left(\theta_2/2\right)\sin(\theta_1)\\ &\quad + \left(\cos^2(k_x)\cos(\theta_1) + \sin^2(k_x)\right)\sin\left(\theta_2/2\right)\\ \sin\left(E_{\theta_1,\theta_2}(k_x,k_y)\right) n_z(\theta_1,\theta_2,k_x,k_y) &= \left(\cos(k_x+2k_y)\cos(\theta_1)\sin(k_x) + \cos(k_x)\sin(k_x+2k_y)\right)\\ &\quad \left(-\cos\left(\theta_2/2\right)\cos(k_x)\sin(k_x)\sin(\theta_1)\sin\left(\theta_2/2\right)\right)\end{aligned}$$

The topological invariant of the system is called the first Chern number. It counts the number of times the unit vector $\vec{n}$ covers the unit sphere as k_x, k_y traverse the Brillouin zone. For a 2×2 Hamiltonian it is defined as:

$$C = \frac{1}{4\pi}\int_{BZ} d^2k \left(\vec{n} \cdot \left(\partial_{k_z}\vec{n} \times \partial_{k_y}\vec{n}\right)\right) \tag{7.4}$$

One can evaluate the first Chern number numerically for $(\theta_1,\theta_2) \in \{-2\pi, 2\pi\}$, Fig. 7.2. The edge states can be probed by iterating Eq. (7.1) on a square lattice, Fig. 7.3.

Phase-Diagram for the 2D split-step protocol

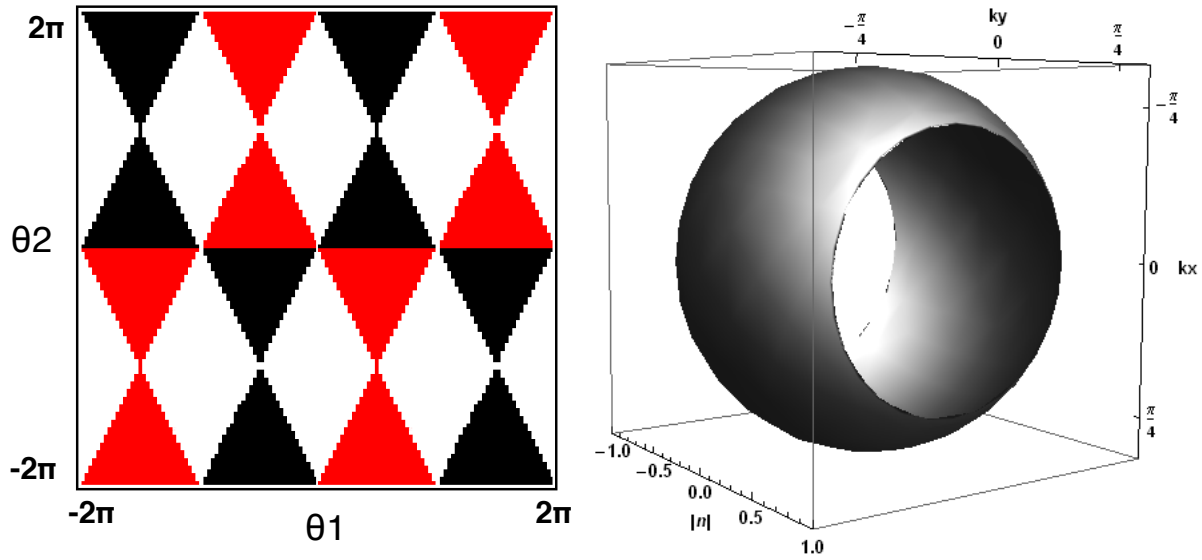

Figure 7.2.: **Left:** Phase-diagram for the 2D split-step quantum walk from Eq. (7.1) obtained through numerical evaluation of Eq. (7.4), screened with intervals of 0.2 width. White(red)(black) regions correspond to a Chern value of $0(-1)(1)$. **Right:** Geometrical interpretation of the Chern number. It counts the number of times the unit vector $\vec{n}$ covers the unit sphere. Parametric plot for $\vec{n}(k_x, k_y, \theta_1, \theta_2)$ with $(\theta_1, \theta_2) = (\pi, \frac{\pi}{2})$ corresponding to a Chern number of 0. In fact, this geometrical object consists of two equal layers with opposite orientation adding up two a winding number of 0.

The angles (θ_1, θ_2) are chosen to be site dependent with:

$$\theta_1(y) = \theta_2(y) = \begin{cases} \frac{3\pi}{2} & (C = -1), \quad 25 \leq y < 75 \\ \frac{7\pi}{6} & (C = 1), \quad \text{else} \end{cases} \tag{7.5}$$

Edge states can be seen best at an atomically sharp boundary.

$$\theta_1(y) = \theta_2(y) = \begin{cases} \frac{3\pi}{2} & (C = -1), \quad y = 25 \vee y = 75 \\ \frac{7\pi}{6} & (C = 1), \quad \text{else} \end{cases} \tag{7.6}$$

In Fig. 7.3 the presence of chiral edge modes and edge states at the spatial boundary of a topological phase can be seen.

Chiral Edge Modes - Quantum Walk on a Square Lattice

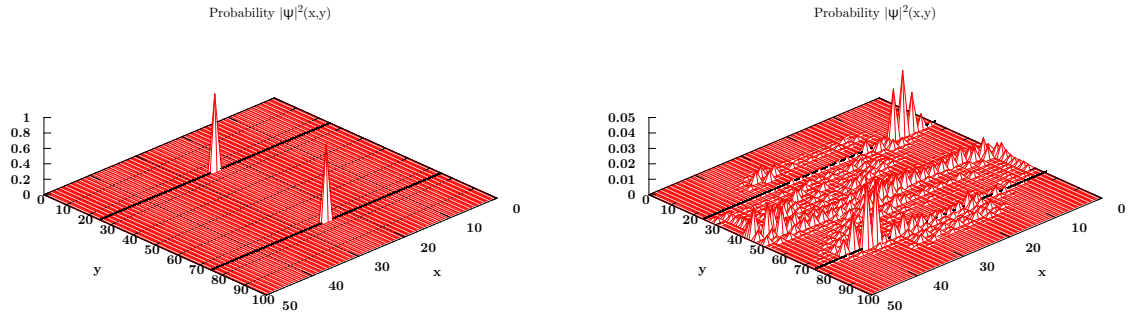

(a) Initial setup $|\Psi\rangle_1 = |x = 25, y = 75\rangle \times |\uparrow\rangle$,$|\Psi\rangle_2 = |x = 25, y = 25\rangle \times |\uparrow\rangle$

(b) 20 Iterations of Eq.(7.1)

Edge States at Phase Boundaries

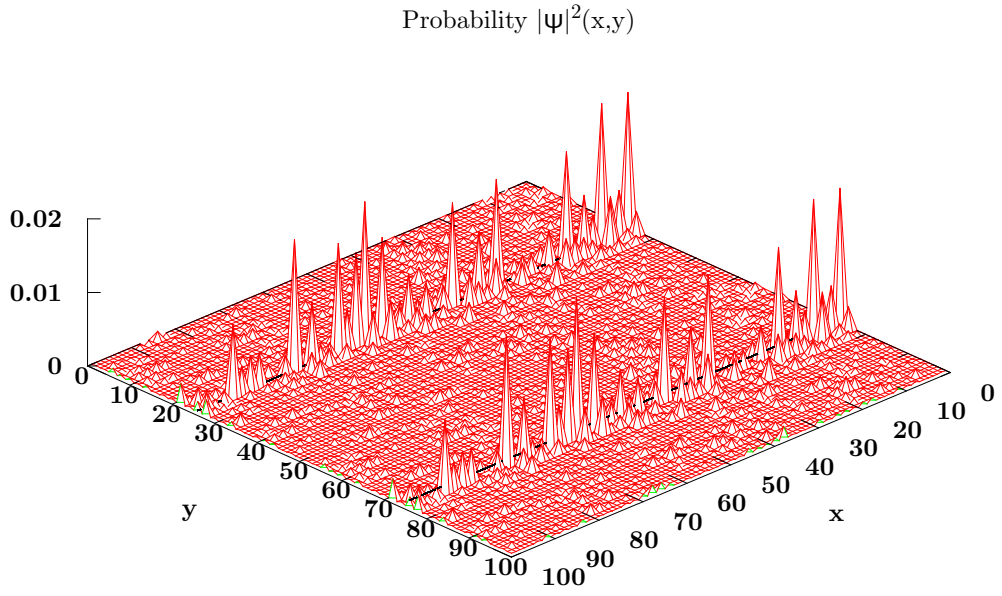

(c) 1000 Iterations of Eq.(7.1)

Figure 7.3.: Quantum Walk on a square lattice (100×100) with grid-length 1 and periodic boundary conditions
Left: Initial position of the walker, placed directly on the phase lines (black)
Right: Probability of presence for the walker after 20 iterations of the 2D split-step protocol. Chiral edge states are propagating into different directions independent of initial spin orientation.
Bottom: Two edge states appear at the phase lines (black). They are present independently of the form of the boundary. They can be seen best with an atomically sharp one, Eq. (7.6)

A. Appendix

List of Figures

List of Tables

δ	A	ΔA	B	ΔB
0.070	0.413	0.004	0.5167	0.0009
0.075	0.324	0.003	0.4872	0.0009
0.080	0.401	0.003	0.5012	0.0006
0.085	0.407	0.003	0.4965	0.0006
0.090	0.458	0.003	0.5019	0.0006
0.095	0.493	0.003	0.5044	0.0006
0.100	0.556	0.006	0.5122	0.0011
0.105	0.478	0.005	0.4915	0.0010
0.110	0.664	0.007	0.5213	0.0011
0.115	0.597	0.006	0.5049	0.0011
0.120	0.643	0.005	0.5080	0.0008
0.125	0.645	0.005	0.5046	0.0008
0.130	0.675	0.003	0.5044	0.0005
0.135	0.647	0.003	0.4965	0.0005
0.140	0.752	0.003	0.5080	0.0004
0.145	0.706	0.003	0.4977	0.0004
0.150	0.792	0.003	0.5067	0.0004
0.155	0.766	0.003	0.5002	0.0004
0.160	0.819	0.003	0.5036	0.0004
0.165	0.831	0.003	0.5018	0.0004
0.170	0.862	0.003	0.5030	0.0004
0.175	0.872	0.003	0.5009	0.0004
0.180	0.972	0.004	0.5098	0.0004
0.185	0.998	0.004	0.5097	0.0004
0.190	0.894	0.003	0.4942	0.0004
0.195	0.994	0.004	0.5031	0.0004
0.200	0.986	0.002	0.4994	0.0003
0.210	1.092	0.003	0.5057	0.0003
0.220	1.069	0.003	0.4976	0.0003
0.230	1.191	0.003	0.5050	0.0003
0.240	1.185	0.003	0.4998	0.0003
0.250	1.284	0.003	0.5041	0.0003
0.260	1.319	0.003	0.5029	0.0003
0.270	1.394	0.004	0.5045	0.0003
0.280	1.384	0.004	0.4996	0.0003
0.290	1.501	0.004	0.5046	0.0003
0.300	1.532	0.004	0.5029	0.0003
Mean Value			0.503	0.001

Table A.1.: Table of coefficients A(δ) and B for the fits of the diffusive tails $n_\delta(t) = A(\delta)t^{-B}$

δ	$\xi = 3, w = 1$ $b[10^5]$	$\Delta b[10^5]$	δ	$\xi = 3, w = 1$ $b[10^5]$	$\Delta b[10^5]$
0.010	0.73928	0.00001	0.130	105.56800	0.07071
0.015	1.67399	0.00002	0.135	111.92500	0.14480
0.020	2.94629	0.00005	0.140	117.86400	0.15600
0.025	4.57673	0.00011	0.145	126.93700	0.15000
0.030	6.49432	0.00035	0.150	132.47800	0.18130
0.035	8.89828	0.00039	0.155	153.03600	0.23310
0.040	11.53160	0.00084	0.160	160.30700	0.27470
0.045	14.31650	0.00138	0.165	171.86300	0.31190
0.050	17.53350	0.00224	0.170	187.14800	0.22930
0.055	21.16770	0.00260	0.175	188.93400	0.34760
0.060	24.92480	0.00480	0.180	195.62700	0.36100
0.065	29.15160	0.00801	0.185	194.29000	0.51680
0.070	33.35950	0.01076	0.195	209.33700	0.58750
0.075	37.80820	0.01310	0.200	218.34400	0.40660
0.080	43.27450	0.01778	0.210	231.24800	0.53000
0.085	48.79910	0.01950	0.220	237.00900	0.46000
0.090	54.28360	0.02429	0.230	267.52000	0.38940
0.095	60.84670	0.02781	0.240	300.11000	1.54000
0.100	65.79650	0.04117	0.250	305.76500	0.85680
0.105	72.97590	0.03679	0.260	342.93600	1.56300
0.110	78.88420	0.04071	0.270	322.11500	1.15400
0.115	86.59870	0.05013	0.280	342.77300	1.18800
0.120	91.12840	0.05169	0.290	357.13900	1.74100
0.125	98.65350	0.08441	0.300	353.32400	1.28400

Table A.2.: Time-constants for the exponential decay of the bound states subject to dynamic disorder with parametric values $\xi = 3$, $w = 1$.

δ	$\xi = 1.5, w = 50$ $b[10^5]$	$\Delta b[10^5]$	$\xi = 1.5, w = 75$ $b[10^5]$	$\Delta b[10^5]$	$\xi = 1.5, w = 100$ b	$\Delta b[10^5]$
0.010	3.362	0.001	2.823	0.001	3.364	0.001
0.015	7.523	0.003	6.460	0.002	7.640	0.002
0.020	13.408	0.004	11.393	0.003	13.386	0.004
0.025	20.952	0.004	18.122	0.006	21.106	0.005
0.030	29.773	0.007	25.845	0.006	30.223	0.009
0.035	40.751	0.009	35.782	0.012	42.255	0.014
0.040	52.442	0.019	46.187	0.012	53.993	0.020
0.045	66.535	0.019	58.628	0.022	68.990	0.020
0.050	82.660	0.021	71.854	0.020	84.536	0.017
0.055	99.266	0.033	89.022	0.027	100.263	0.023
0.060	120.078	0.052	103.951	0.038	121.285	0.023
0.065	138.827	0.046	123.755	0.026	142.308	0.029
0.070	161.749	0.096	142.597	0.046	160.968	0.059
0.075	184.619	0.074	162.826	0.049	181.917	0.065
0.080	207.512	0.118	185.522	0.036	210.524	0.083
0.085	234.170	0.101	209.722	0.066	233.667	0.093
0.090	257.177	0.125	233.365	0.095	260.345	0.108
0.095	291.635	0.107	260.618	0.171	295.246	0.082
0.100	321.196	0.236	295.754	0.181	324.939	0.150
0.105	354.529	0.217	323.837	0.112	356.361	0.276
0.110	383.928	0.337	356.662	0.220	386.130	0.212
0.115	420.208	0.362	386.090	0.309	419.662	0.138
0.120	452.743	0.328	414.959	0.232	457.238	0.290
0.125	493.670	0.472	458.972	0.327	476.481	0.362
0.130	527.789	0.657	492.745	0.286	525.191	0.357
0.135	585.085	0.593	525.676	0.618	584.950	1.158
0.140	613.960	1.035	568.927	0.457	634.598	1.423
0.145	658.327	1.284	625.248	0.546	677.436	1.289
0.150	732.057	2.688	658.188	0.989	716.064	1.412
0.160	830.451	3.784	753.188	1.154	811.334	1.408
0.170	916.307	3.503	842.187	1.325	894.940	2.709
0.180	987.350	4.678	926.749	1.045	987.476	2.196
0.190	1063.610	3.904	1044.940	2.841	1084.130	1.758
0.200	1188.910	5.619	1120.280	1.888	1170.430	2.945

Table A.3.: Time-constants for the exponential decay of the bound states subject to dynamic disorder with parametric values $\xi = 1.5$, $w = 50, 75, 100$.

δ	$\xi = 3, w = 50$ $b[10^5]$	$\Delta b[10^5]$	$\xi = 3, w = 50$ $b[10^5]$	$\Delta b[10^5]$	$\xi = 3, w = 50$ b	$\Delta b[10^5]$
0.010	5.99	0.01	6.68	0.004	5.37	0.01
0.015	11.65	0.02	12.58	0.021	12.22	0.01
0.020	18.50	0.04	20.38	0.030	22.73	0.02
0.025	24.34	0.04	29.89	0.056	32.11	0.04
0.030	32.74	0.08	39.28	0.104	44.21	0.10
0.035	39.18	0.05	50.76	0.080	62.59	0.09
0.040	49.78	0.05	70.64	0.134	79.88	0.21
0.045	62.42	0.05	75.15	0.066	91.57	0.15
0.050	78.07	0.06	94.79	0.091	120.22	0.18
0.055	92.51	0.03	120.70	0.163	145.09	0.45
0.060	108.68	0.03	142.04	0.234	165.61	0.28
0.065	128.50	0.05	160.73	0.428	191.30	0.18
0.070	152.16	0.15	190.92	0.282	206.00	0.35
0.075	174.42	0.18	202.51	0.366	237.45	0.36
0.080	191.20	0.09	230.92	0.232	285.95	0.48
0.085	214.11	0.15	270.35	0.381	313.09	0.54
0.090	243.34	0.07	291.81	0.241	337.45	0.52
0.095	284.10	0.38	325.07	0.470	396.07	0.38
0.100	305.45	0.32	378.63	1.367	427.27	0.64
0.105	336.61	0.43	399.72	0.963	456.15	0.60
0.110	376.12	0.49	439.50	1.564	507.15	1.39
0.115	396.26	0.77	472.59	1.518	563.64	0.61
0.120	424.30	0.82	504.42	1.446	597.56	1.13
0.125	474.26	0.81	592.64	3.649	654.74	1.59
0.130	505.30	1.11	622.61	4.257	671.07	1.39
0.135	547.91	1.08	695.19	5.408	786.17	2.78
0.140	581.20	1.24	728.83	5.102	823.25	1.64
0.145	603.47	2.82	805.48	6.897	852.75	2.21
0.150	647.90	1.70	840.54	6.093	945.50	4.38
0.160	790.06	1.96	908.30	5.367	988.69	2.64
0.170	868.25	3.54	990.54	6.855	1077.01	2.91
0.180	986.24	3.99	1068.72	7.639	1180.54	4.54
0.190	1065.80	3.88	1146.78	8.430	1281.02	5.32
0.200	1084.49	4.89	1255.21	9.614	1325.06	5.56

Table A.4.: Time-constants for the exponential decay of the bound states subjected to dynamic disorder with parametric values $\xi = 3$, $w = 50, 75, 100$.

δ	$\xi = 4.5, w = 50$ $b[10^5]$	$\Delta b[10^5]$	$\xi = 4.5, w = 75$ $b[10^5]$	$\Delta b[10^5]$	$\xi = 4.5, w = 100$ b	$\Delta b[10^5]$
0.010	7.99	0.02	9.31	0.04	11.80	0.06
0.015	14.72	0.04	15.15	0.08	16.88	0.13
0.020	24.26	0.04	19.87	0.10	21.77	0.19
0.025	38.82	0.04	28.80	0.10	25.33	0.17
0.030	50.10	0.07	38.74	0.09	33.19	0.18
0.035	66.59	0.05	51.29	0.10	41.35	0.15
0.040	86.88	0.06	66.61	0.07	51.03	0.16
0.045	109.05	0.05	79.14	0.04	61.50	0.16
0.050	133.39	0.05	104.89	0.06	75.60	0.25
0.055	159.00	0.09	125.41	0.10	89.66	0.23
0.060	195.55	0.14	162.65	0.09	102.50	0.25
0.065	234.50	0.36	172.87	0.10	113.17	0.23
0.070	247.46	0.16	204.94	0.10	135.54	0.31
0.075	264.04	0.39	231.11	0.06	151.02	0.38
0.080	349.83	0.41	271.91	0.16	175.37	0.36
0.085	365.34	0.29	300.78	0.14	195.37	0.43
0.090	397.43	0.65	338.05	0.31	211.89	0.36
0.095	470.20	0.48	379.12	0.42	268.79	1.09
0.100	515.51	1.09	404.57	0.20	296.22	1.02
0.105	540.24	1.91	470.88	0.77	331.31	1.10
0.110	634.73	4.11	499.36	0.53	355.78	1.23
0.115	712.18	4.15	529.76	0.99	389.18	1.11
0.120	768.35	3.63	592.51	0.80	412.84	1.23
0.125	819.55	3.78	704.01	4.29	435.29	1.40
0.130	872.12	4.46	762.73	4.00	496.73	1.62
0.135	941.16	6.26	780.58	4.60	578.43	2.87
0.140	994.94	8.80	786.09	5.51	620.90	3.88
0.145	1021.38	10.07	867.72	4.99	658.77	3.52
0.150	1205.34	15.12	998.48	7.59	700.38	3.22
0.160	1324.28	16.89	1080.62	8.75	785.42	3.43
0.170	1352.51	16.87	1140.49	9.16	863.93	4.15
0.180	1538.51	24.45	1199.86	9.20	960.98	5.91
0.190	1608.95	20.23	1343.35	12.93	1034.98	6.10
0.200	1693.63	21.46	1377.57	13.08	1162.33	6.33

Table A.5.: Time-constants for the exponential decay of the bound states subjected to dynamic disorder with parametric values $\xi = 4.5$, $w = 50, 75, 100$.

δ	$\xi = 6, w = 50$ $b[10^5]$	$\Delta b[10^5]$	$\xi = 6, w = 75$ $b[10^5]$	$\Delta b[10^5]$	$\xi = 6, w = 100$ b	$\Delta b[10^5]$
0.010	9.84	0.01	11.14	0.02	12.12	0.03
0.015	16.48	0.04	20.54	0.06	23.06	0.06
0.020	24.82	0.06	25.33	0.10	34.04	0.15
0.025	30.69	0.06	33.21	0.13	47.51	0.23
0.030	40.95	0.08	39.70	0.09	56.89	0.30
0.035	53.48	0.07	52.53	0.10	78.90	0.33
0.040	66.81	0.08	64.85	0.06	89.03	0.31
0.045	80.72	0.07	84.34	0.08	112.16	0.30
0.050	102.56	0.03	99.89	0.08	141.42	0.17
0.055	116.57	0.05	124.38	0.11	158.73	0.30
0.060	151.90	0.20	148.92	0.12	193.41	0.19
0.065	182.08	0.32	171.80	0.05	221.19	0.15
0.070	194.52	0.28	205.30	0.12	244.63	0.22
0.075	215.92	0.18	233.31	0.15	278.80	0.21
0.080	243.10	0.40	259.81	0.14	314.38	0.16
0.085	265.26	0.43	302.26	0.16	364.21	0.31
0.090	284.12	0.48	333.62	0.27	412.13	0.42
0.095	366.12	1.10	343.49	0.16	468.57	0.52
0.100	398.63	1.20	417.37	0.29	522.71	0.62
0.105	429.09	1.01	427.64	0.74	542.63	0.48
0.110	466.28	1.00	480.31	0.43	556.02	0.83
0.115	497.09	2.32	507.08	0.63	650.90	0.56
0.120	563.86	2.86	569.38	0.87	730.98	6.37
0.125	605.17	3.53	601.51	1.20	817.58	6.35
0.130	633.04	4.83	645.31	1.76	848.92	6.61
0.135	699.13	4.98	741.07	2.36	916.07	7.45
0.140	720.10	5.13	788.65	4.22	966.32	7.23
0.145	851.89	10.31	785.32	3.29	986.61	6.39
0.150	894.08	10.31	950.77	9.33	1083.21	9.07
0.160	977.36	24.87	1026.19	9.25	1182.81	9.57
0.170	1065.41	11.86	1113.24	9.32	1325.81	9.49
0.180	1108.39	29.02	1190.67	10.97	1380.75	9.76
0.190	1161.81	13.26	1235.15	9.88	1523.05	13.21
0.200	1240.19	14.65	1328.87	11.43	1602.22	14.44

Table A.6.: Time-constants for the exponential decay of the bound states subjected to dynamic disorder with parametric values $\xi = 6$, $w = 50, 75, 100$.

Bibliography

[1] Kitagawa, Takuya ; Rudner, Mark S. ; Berg, Erez ; Demler, Eugene: Exploring topological phases with quantum walks. In: *Phys. Rev. A* 82 (2010), Sep, 033429. http://dx.doi.org/10.1103/PhysRevA.82.033429. – DOI 10.1103/PhysRevA.82.033429

[2] Schnyder, Andreas P. ; Ryu, Shinsei ; Furusaki, Akira ; Ludwig, Andreas W. W.: Classification of topological insulators and superconductors in three spatial dimensions. In: *Phys. Rev. B* 78 (2008), Nov, 195125. http://dx.doi.org/10.1103/PhysRevB.78.195125. – DOI 10.1103/PhysRevB.78.195125

[3] Childs, Andrew M. ; Farhi, Edward ; Gutmann, Sam: An Example of the Difference Between Quantum and Classical Random Walks. In: *Quantum Information Processing* 1 (2002), April, Nr. 1, 35–43. http://dx.doi.org/10.1023/A:1019609420309. – DOI 10.1023/A:1019609420309

[4] Kane, C. L. ; Mele, E. J.: Quantum Spin Hall Effect in Graphene. In: *Phys. Rev. Lett.* 95 (2005), Nov, 226801. http://dx.doi.org/10.1103/PhysRevLett.95.226801. – DOI 10.1103/PhysRevLett.95.226801

[5] Bernevig, B. A. ; Hughes, Taylor L. ; Zhang, Shou-Cheng: Quantum Spin Hall Effect and Topological Phase Transition in HgTe Quantum Wells. In: *SCIENCE* 314 (2006), 1757. doi:10.1126/science.1133734

[6] König, Markus ; Wiedmann, Steffen ; Brüne, Christoph ; Roth, Andreas ; Buhmann, Hartmut ; Molenkamp, Laurens W. ; Qi, Xiao-Liang ; Zhang, Shou-Cheng: Quantum Spin Hall Insulator State in HgTe Quantum Wells. In: *Science* 318 (2007), November, Nr. 5851, 766–770. http://dx.doi.org/10.1126/science.1148047. – DOI 10.1126/science.1148047

[7] Kane, Charles L.: Condensed matter: An insulator with a twist. In: *Nat Phys* 4 (2008), Mai, Nr. 5, 348–349. http://dx.doi.org/10.1038/nphys955. – DOI 10.1038/nphys955

[8] Fu, Liang ; Kane, C. L.: Superconducting Proximity Effect and Majorana Fermions at the Surface of a Topological Insulator. In: *Phys. Rev. Lett.* 100 (2008), Mar, 096407. http://dx.doi.org/10.1103/PhysRevLett.100.096407. – DOI 10.1103/PhysRevLett.100.096407

[9] Fahri, Gutmann S. E.: Quantum Computation and Decision Trees. (1997). http://dx.doi.org/10.1103/PhysRevA.58.915. – DOI 10.1103/PhysRevA.58.915

[10] Kempe, J: Quantum random walks: An introductory overview. In: *Contemporary Physics* 44 (2003), Nr. 4, 307-327. http://dx.doi.org/10.1080/00107151031000110776. – DOI 10.1080/00107151031000110776

[11] Kane, Charles L. ; Mele, Eugene J.: A New Spin on the Insulating State. In: *Science* 314 (2006), Dezember, Nr. 5806, 1692–1693. http://dx.doi.org/10.1126/science.1136573. – DOI 10.1126/science.1136573

[12] Electrons in New Guises. (1998). http://www.nobelprize.org/nobel_prizes/physics/laureates/1998/press.html. – last pageview : 22nd January, 2012

[13] Furusaki, Akira: *Topological Insulators*. Lecture Notes - 4th February , 2009. http://www.riken.go.jp/lab-www/theory/colloquium/. Version: 2009. – last pageview : 22nd January, 2012

[14] Hasan, M. Z.: *Quantum Spin Hall Effect and Topological Insulators*. Lecture Notes - Princeton Summer School on Condensed Matter Physics 2008. http://www.physics.princeton.edu/~claumann/summerschool2008/Princeton%20Summer%20School%20on%20Condensed%20Matters%20Physics%202008.html. Version: 2008. – last pageview : 22nd January, 2012

[15] Moore, Joel: *MIT minicourse "Recent developments in topological phases"*. Lecture Notes - 18-20 January , 2011. http://socrates.berkeley.edu/~jemoore/Moore_group,_UC_Berkeley/Welcome_to_the_Moore_group,_Department_of_Physics,_UC_Berkeley.html. Version: January 2011. – last pageview : 22nd January, 2012

[16] Moore, J. E.: The birth of topological insulators. In: 464 (2010), März, S. 194–198. http://dx.doi.org/10.1038/nature08916. – DOI 10.1038/nature08916

[17] Hasan, M ; Kane, C: Colloquium: Topological insulators. In: *Reviews of Modern Physics* 82 (2010), Nr. 4, 3045–3067. http://link.aps.org/doi/10.1103/RevModPhys.82.3045

[18] Berry, M. V.: Quantal Phase Factors Accompanying Adiabatic Changes. In: *Proceedings of the Royal Society of London. Series A, Mathematical and Physical Sciences* 392 (1984), Nr. 1802, 45–57. http://dx.doi.org/10.2307/2397741. – DOI 10.2307/2397741. – ISSN 00804630

[19] Schwabl, F.: *Springer-Lehrbuch*. Bd. 5: *Quantenmechanik für Fortgeschrittene (QM II)*. Springer Berlin, 2008 http://books.google.de/books?id=C8lJewAACAAJ. – ISBN 9783540850762

[20] Su, W. P. ; Schrieffer, J. R. ; Heeger, A. J.: Solitons in Polyacetylene. In: *Phys. Rev. Lett.* 42 (1979), Jun, 1698–1701. http://dx.doi.org/10.1103/PhysRevLett.42.1698. – DOI 10.1103/PhysRevLett.42.1698

[21] Michael Karski, Jai-Min Choi Andreas Steffen Wolfgang Alt Dieter Meschede Artur W. Leonid Förster F. Leonid Förster: Quantum Walk in Position Space with Single Optically Trapped Atoms. (2009), July. http://arxiv.org/abs/0907.1565v1

[22] Andre Ahlbrecht, Dieter Meschede Volkher B. Scholz Albert H. Werner Reinhard F. W. Andrea Alberti A. Andrea Alberti: Bound Molecules in an Interacting Quantum Walk. (2011), May. http://arxiv.org/abs/1105.1051v1

[23] Qi, Xiao-Liang ; Hughes, Taylor L. ; Zhang, Shou-Cheng: Topological field theory of time-reversal invariant insulators. In: *Phys. Rev. B* 78 (2008), Nov, 195424. http://dx.doi.org/10.1103/PhysRevB.78.195424. – DOI 10.1103/PhysRevB.78.195424

[24] Zhang, Shou-cheng: Topological states of quantum matter. In: *Physics* 1 (2008), Jul, 6. http://dx.doi.org/10.1103/Physics.1.6. – DOI 10.1103/Physics.1.6

[25] Ryu, Shinsei ; Hatsugai, Yasuhiro: Topological Origin of Zero-Energy Edge States in Particle-Hole Symmetric Systems. In: *Phys. Rev. Lett.* 89 (2002), Jul, 077002. http://dx.doi.org/10.1103/PhysRevLett.89.077002. – DOI 10.1103/PhysRevLett.89.077002

[26] Kane, C.L. ; Moore, J.E.: Topological insulator. In: *Physics World* 24 (2011)

B. Declaration and Acknowledgements

Acknowledgment

I acknowledge the support from Christoph Schütte, especially for his introduction into `C++` programming.
Moreover, I would like to thank Matthias Sitte for his assistance in numerics.
Both Matthias and Christoph always took time for me and cared for my problems. I am thankful for their suggestions, discussions and comments on my Bachelor Thesis. I appreciate very much that Professor Achim Rosch gave me the opportunity to write a Bachelor Thesis on my favourite topic 'Quantum Walks', providing me an insight into up-to-date research of theoretical physics. The work on the Thesis was both challenging and rewarding. Moreover, I am thankful for being well-received by the working groups of the Institute of Theoretical Physics, making it a pleasant and stimulating working experience.

Declaration

I hereby declare that I wrote my thesis "Time-Dependent Disorder in a Topological Insulator Realised with a Quantum Walk" without any unlawful aids. I further declare that to the best of my knowledge and belief all external authorships have been correctly cited and marked as such.

_____

Jan Gelhausen, Cologne, January 26, 2012